NASA CONTRACTOR REPORT

NASA CR-830

NASA CR-8

ANALYSIS AND DESIGN OF SPACE VEHICLE FLIGHT CONTROL SYSTEMS

VOLUME XI - COMPONENT DYNAMICS

by J. G. Rolland Collette

Prepared by
GENERAL DYNAMICS CORPORATION
San Diego, Calif.
for George C. Marshall Space Flight Center

NATIONAL AERONAUTICS AND SPACE ADMINISTRATION • WASHINGTON, D. C. • JULY 1967

NASA CR-830

ANALYSIS AND DESIGN OF SPACE VEHICLE FLIGHT CONTROL SYSTEMS

VOLUME XI - COMPONENT DYNAMICS

By J. G. Rolland Collette

Issued by Originator as GDC-DDE66-031

Prepared under Contract No. NAS 8-11494 by
GENERAL DYNAMICS CONVAIR
A DIVISION OF GENERAL DYNAMICS CORPORATION
San Diego, Calif.

for George C. Marshall Space Flight Center

NATIONAL AERONAUTICS AND SPACE ADMINISTRATION

For sale by the Clearinghouse for Federal Scientific and Technical Information
Springfield, Virginia 22151 – CFSTI price $3.00

FOREWORD

This report was prepared under NASA Contract NAS 8-11494 and is one of a series intended to illustrate methods used for the design and analysis of space vehicle flight control systems. Below is a complete list of the reports in the series:

Volume I	Short Period Dynamics
Volume II	Trajectory Equations
Volume III	Linear Systems
Volume IV	Nonlinear Systems
Volume V	Sensitivity Theory
Volume VI	Stochastic Effects
Volume VII	Attitude Control During Launch
Volume VIII	Rendezvous and Docking
Volume IX	Optimization Methods
Volume X	Man in the Loop
Volume XI	Component Dynamics
Volume XII	Attitude Control in Space
Volume XIII	Adaptive Control
Volume XIV	Load Relief
Volume XV	Elastic Body Equations
Volume XVI	Abort

The work was conducted under the direction of Clyde D. Baker, Billy G. Davis and Fred W. Swift, Aero-Astro Dynamics Laboratory, George C. Marshall Space Flight Center. The General Dynamics Convair program was conducted under the direction of Arthur L. Greensite.

TABLE OF CONTENTS

LIST OF ILLUSTRATIONS

LIST OF ILLUSTRATIONS (Contd)

1. STATEMENT OF THE PROBLEM

The operation of a control system consists of three elemental processes representing the basic functions to be performed: sensing, signal-processing, and actuation. Each process can be carried out by any of a large number of elements that are generally classified into groups according to the function involved. A sensing element senses or measures some absolute or relative physical variable. An actuating element provides control action; it refers to the signal that activates a system to produce a desired motion.

Signal processing generally refers to the conditioning and adaptation of flight program, celestial attitude, guidance, and navigation signals to the flight control system. The processing can be carried out by computers on board the vehicle or at some remote point from which it can be transmitted to the vehicle via data links. This subject, which is primarily one of applying proper coordinate transformations between signal loops, is excluded from the present discussion. Coordinate transformations in the context of launch vehicle guidance and control are discussed in Ref. 16.

In addition, the number, complexity, and possible applications of the elements included in the broad categories of sensing and actuation are such that a reasonable discussion of each can not be included here. Of immediate concern are only those elements most extensively used in: measuring reference and stabilizing inputs to the controlled systems (launch vehicles); and actuating the prime movers that control these systems. The sensing elements discussed are gyroscopes, accelerometers, platforms, and angle-of-attack sensors; actuating elements are those utilizing electrical, pneumatic, and hydraulic power. A combination fairly representative of the state of the art in attitude control consists of gyroscopic instruments for sensing and electrohydraulic units for actuation. These components have therefore been singled out for more extensive treatment.

The purposes of the monograph are to present the formulation of mathematical models for these sensors and actuators, applicable throughout the frequency range of interest, and to account for phenomena that can influence the results of analyses. Some of these phenomena are inherent in the operation of the hardware and should be recognized as such. Others can be avoided or minimized by imposing constraints on the design of equipment and/or on its installation. Therefore some functional requirements are included in the discussion.

The linear transfer function representation of inherently nonlinear systems often yields results having no real quantitative significance. Usually, more meaningful analyses can be performed with "equivalent linear" transfer functions that include nonlinear characteristics as reflected by describing functions. The derivation of such a

describing function is presented, and the results are applied to an electrohydraulic position servo. Its usefulness in predicting stability characteristics is described in more detail in another monograph in this series (Vol. III, part I, Attitude Control During Launch).

2. STATE OF THE ART

In the multiloop, multichannel feedback flight control systems of launch vehicles, sensors provide data inputs to which the systems should respond. Of all the physical variables used to describe the performance of the vehicles, only a few are used as primary references for stabilizing purposes. Angular rates have found almost universal acceptance as the basic variables in stabilization networks. These rates, measured or derived, are usually coupled to attitude references to form the primary inputs to attitude control loops. Some secondary or auxiliary quantities, such as linear accelerations and angle of attack, or sideslip, are used where compensation or alleviation of certain conditions is required.

A large variety of instruments has been devised to measure these variables. Although optical, radar, and other noninertial devices can be used either as references or to monitor references, present-day sensing for stabilization consists almost entirely of inertial electromechanical instrumentation. The rotating-mass gyroscope, with constraints tailored for the quantity to be measured, is still the mainstay for angular measurements. The seismic-mass, force-balance, and gyro-pendulum accelerometers and their derivatives are widely used for linear quantities. Combinations of these instruments are exemplified by the inertial platform, which forms the heart of most contemporary guidance systems and provides a good attitude reference. Angle-of-attack sensing is being done largely through pressure-differential measurements, although the simple aerodynamic vane is still called upon for some applications.

The approximate transfer functions for these sensors have been established well enough to predict performance on a satisfactory basis. Improvements in mathematical representation has come mostly through better understanding of the "false" signals the equipment can generate and the description, and inclusion where appropriate, of these signals in the analyses of systems. Attempts to minimize these spurious signals are made through specification of functional requirements in hardware design and installation.

To some extent, sensing technology can be said to be on the threshold of transition. New discoveries, especially in the field of solid-state physics, are constantly being applied to the design of precision mechanisms. New instruments that take advantage of the perfect inertial properties of atomic nuclei, of the nature of electrical resistance near absolute zero, or of some absolute constant such as the velocity of light have been conceived. Still in various stages of experimentation, these instruments indicate great potential for the not-too-distant future.

Control elements are defined as those prime movers, such as aerodynamic surfaces and gimballed engines, that provide the forces and moments to stabilize and control vehicles. The actuating elements are the system components that activate the prime movers in response to commands from the sensing and guiding elements.

The control system must meet both steady-state and transient performance criteria of power and accuracy. Practical considerations of control loads, weight and space, etc., lead to high power/weight and power/volume ratio requirements for relatively precise motion control. Continuous variation of controlled parameters, such as large torques, velocities, and positions, must be achieved easily and rapidly with precision. To provide the required performance within the allotted system weight, space, and cost, hydraulic power (represented by electrohydraulic servo units) has been the overwhelming choice of designers, regardless of the method of control employed.

To determine the characteristics of a servo system, the behavior of the components should be known and formulated in terms that describe their operation singly and/or in combination with others. Control and environmental characteristics that influence the performance of the servo unit must also be delineated and incorporated in the overall representation of the system. Most of the problems attendant to good mathematical modeling of the hardware stem from the nonlinear nature of its operation; other nonlinearities (structural deformation, control friction, etc.) only emphasize the difficulties. Therefore, the formulation of a model usually involves some compromise. Semi-analytical tools such as the phase plane and describing functions have been successfully applied to obtain good approximations to system behavior. Computers, of course, have given us the ability to simulate nonlinear characteristics with some accuracy. This has allowed us to verify the validity of analyses and to refine designs without compromising the actual systems.

3. RECOMMENDED PROCEDURES

3.1 SENSING ELEMENTS

3.1.1 Gyroscopes

An operating angular momentum gyroscope has two fundamental properties based on Newton's laws of motion:

a. Its momentum vector tends to maintain its inertial orientation.

b. It senses the magnitude and direction of a disturbance.

The inputs and outputs of a gyroscope are commonly described by three mutually associated axes, as shown in Fig. 1. Applying a disturbing torque along either of the two axes transverse to the spin axis results in a motion (precession) that tends to align the spin axis with the direction of the applied torque. This precession law is reversible in that a motion input results in a torque output.

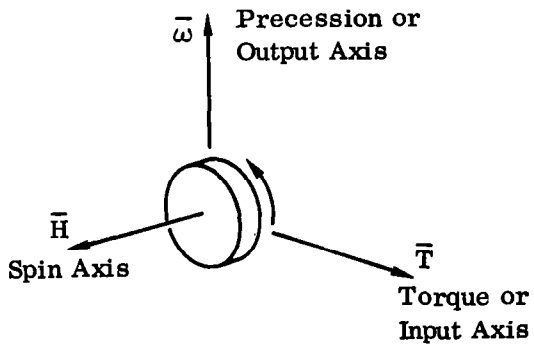

Figure 1. Axes of Gyroscope

Applied to rotational motion, Newton's second law states:

$$\bar{T} = J\left(\frac{d\bar{\omega}}{dt}\right)_I = \left(\frac{d\bar{H}}{dt}\right)_I \qquad (1)$$

where $\bar{T}$ is an applied torque vector

J is the moment of inertia

$\bar{\omega}$ is angular velocity

$\bar{H}$ is the angular momentum

If a body is rotating, with angular momentum $\bar{H}$, with respect to a noninertial frame of reference, "f," which has an inertial angular velocity, $\bar{\omega}_f$, the time rate of change of $\bar{H}$ referred to inertial space is given by

$$\left(\frac{d\bar{H}}{dt}\right)_I = \left(\frac{d\bar{H}}{dt}\right)_f + \left[\bar{\omega}_f \times \bar{H}\right] = \bar{T} \tag{2}$$

or

$$\left[\frac{d(\bar{H})_f}{dt}\right]_I = \left[\frac{d(\bar{H})_f}{dt}\right]_f + \left[(\omega_f)_I \times (\bar{H})_f\right] = \bar{T} \tag{2a}$$

where the subscript I indicates "with respect to inertial space" and
f indicates "with respect to noninertial frame of reference."

Gyroscopes are generally classified in terms of the measurements they provide; e.g., rate gyros and directional gyros. They can also be classified by the number of restraints imposed upon the rotor spin axis (momentum vector). Thus a gyro supported by two gimbals can have its orientation specified through two angular coordinates, usually given by the gimbal positions. Such a gyro is said to have two degrees of freedom (TDOF).

Fig. 2 shows schematically the basic features of a TDOF gyro. Four sets of orthogonal axes (x, y, and z) are defined, with their origins located in 1) inertial space; 2) the gyro case or platform; 3) the outer gimbal, and 4) the inner gimbal. All coordinate systems are assumed to have a common origin and are treated as such.

To relate the four systems to each other, the platform axes are first carried into the inertial frame of reference by successive Euler angle rotations (ϕ_x, ϕ_y, and ϕ_z) about the x axis, the displaced y axis, and the resulting z axis respectively. This results in the direction cosine matrix:

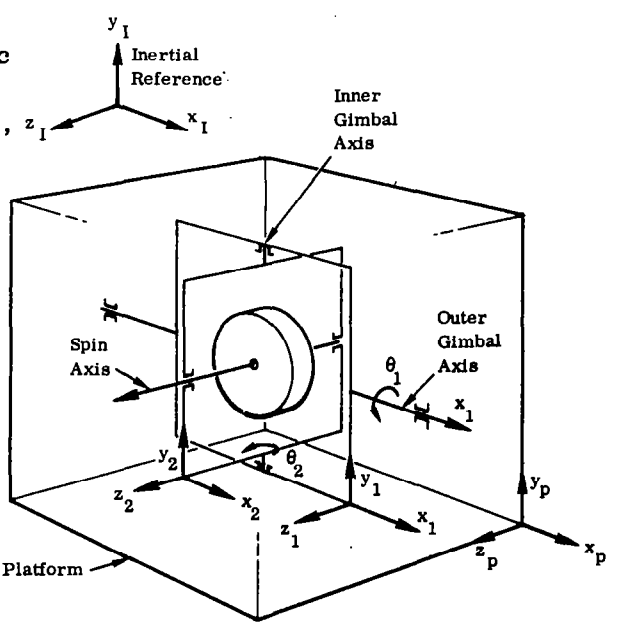

Figure 2. Basic Features of TDOF Gyro

$$\begin{bmatrix} x_I \\ y_I \\ z_I \end{bmatrix} = \begin{bmatrix} \cos\phi_y \cos\phi_z, & \cos\phi_x \sin\phi_z + \sin\phi_x \sin\phi_y \cos\phi_z, & \sin\phi_x \sin\phi_z - \cos\phi_x \sin\phi_y \cos\phi_z \\ -\cos\phi_y \sin\phi_z, & \cos\phi_x \cos\phi_z - \sin\phi_x \sin\phi_y \sin\phi_z, & \sin\phi_x \cos\phi_z + \cos\phi_x \sin\phi_y \sin\phi_z \\ \sin\phi_y, & -\sin\phi_x \cos\phi_y, & \cos\phi_x \cos\phi_y \end{bmatrix} \begin{bmatrix} x_p \\ y_p \\ z_p \end{bmatrix} \quad (3)$$

Using the $\sin\phi = \phi$ and $\cos\phi = 1$ approximations for small angles, we obtain the following transformation.

$$\begin{bmatrix} x_I \\ y_I \\ z_I \end{bmatrix} = \begin{bmatrix} 1 & \phi_z & -\phi_y \\ -\phi_z & 1 & \phi_x \\ \phi_y & -\phi_x & 1 \end{bmatrix} \begin{bmatrix} x_p \\ y_p \\ z_p \end{bmatrix} \quad (4)$$

Next the outer gimbal system (x_1, y_1, z_1) is related to the platform by the single rotation, θ_1, about the x_p axis.

$$\begin{bmatrix} x_p \\ y_p \\ z_p \end{bmatrix} = \begin{bmatrix} 1 & 0 & 0 \\ 0 & \cos\theta_1 & \sin\theta_1 \\ 0 & -\sin\theta_1 & \cos\theta_1 \end{bmatrix} \begin{bmatrix} x_1 \\ y_1 \\ z_1 \end{bmatrix} \quad (5)$$

The pickoff angle, θ_1, is usually servocontrolled to a small enough value to allow Eq. (5) to be written as a small-angle transfer matrix.

$$\begin{bmatrix} x_p \\ y_p \\ z_p \end{bmatrix} = \begin{bmatrix} 1 & 0 & 0 \\ 0 & 1 & \theta_1 \\ 0 & -\theta_1 & 1 \end{bmatrix} \begin{bmatrix} x_1 \\ y_1 \\ z_1 \end{bmatrix} \quad (6)$$

Similarly, the rotation, θ_2, of the inner-gimbal system (x_2,y_2,z_2) about the outer-gimbal y_1 axis yields the following relationship for the two gimbal systems:

$$\begin{bmatrix} x_1 \\ y_1 \\ z_1 \end{bmatrix} = \begin{bmatrix} \cos\theta_2 & 0 & -\sin\theta_2 \\ 0 & 1 & 0 \\ \sin\theta_2 & 0 & \cos\theta_2 \end{bmatrix} \begin{bmatrix} x_2 \\ y_2 \\ z_2 \end{bmatrix} \quad (7)$$

and small-valued θ_2 gives

$$\begin{bmatrix} x_1 \\ y_1 \\ z_1 \end{bmatrix} = \begin{bmatrix} 1 & 0 & -\theta_2 \\ 0 & 1 & 0 \\ \theta_2 & 0 & 1 \end{bmatrix} \begin{bmatrix} x_2 \\ y_2 \\ z_2 \end{bmatrix} \tag{8}$$

Other transformations between these coordinate systems can be obtained by the multiplication and/or inversion of two or more transfer matrices.

The angular velocity of the platform, $\bar{\omega}_p$, is defined in terms of its components.

$$\bar{\omega}_p = \bar{x}_p \omega_x + \bar{y}_p \omega_y + \bar{z}_p \omega_z \tag{9}$$

$$= \bar{\omega}_{px} + \bar{\omega}_{py} + \bar{\omega}_{pz} \tag{9a}$$

The value of $\bar{\omega}_p$ relative to the inertial system can be obtained by starting from the inertial axes and backing through the Euler angle transformation with rates $-\dot{\phi}_z$ about the z_I axis, $-\dot{\phi}_y$ about the intermediate y axis, and $-\dot{\phi}_x$ about the original x_p axis. This expression can be written

$$\bar{\omega}_p = \bar{z}_I \left(-\dot{\phi}_z\right) + \bar{y}' \left(-\dot{\phi}_y\right) + \bar{x}_p \left(-\dot{\phi}_x\right) \tag{10}$$

where $\bar{y}'$ is a unit vector in the direction of the intermediate y axis, representing the second rotation in the Euler angle transformation.

$$\bar{y}' = y_p \cos \phi_x + z_p \sin \phi_x \tag{10a}$$

Inserting $\bar{z}_I$ from the direction cosine matrix, Eq. (3), and the value of $\bar{y}'$, Eq. (10a), into Eq. (10) yields an expression of the form stated in Eq. (9), where, in matrix notation,

$$\begin{bmatrix} \omega_{px} \\ \omega_{py} \\ \omega_{pz} \end{bmatrix} = \begin{bmatrix} -1 & 0 & -\sin \phi_y \\ 0 & -\cos \phi_x & \sin \phi_x \cos \phi_y \\ 0 & -\sin \phi_x & -\cos \phi_x \cos \phi_y \end{bmatrix} \begin{bmatrix} \dot{\phi}_x \\ \dot{\phi}_y \\ \dot{\phi}_z \end{bmatrix} \tag{11}$$

Again assuming small angles and neglecting their second-order terms,

$$\begin{aligned} \omega_{px} &= -\dot{\phi}_x - \dot{\phi}_z \phi_y \\ \omega_{py} &= -\dot{\phi}_y - \dot{\phi}_z \phi_x \\ \omega_{pz} &= -\dot{\phi}_z - \dot{\phi}_y \phi_x \end{aligned} \tag{12}$$

The angular velocity of the outer gimbal, $\bar{\omega}_1$, referred to inertial space, is that of the platform less that of the gimbal relative to the platform.

$$\bar{\omega}_1 = \bar{\omega}_p - \bar{x}_1 \dot{\theta}_1 \tag{13}$$

Using Eq. (5), $\bar{\omega}_p$, as given by Eq. (11), can be transformed into the outer gimbal system. Substitution of the results into Eq. (13) gives an expression of the form

$$\bar{\omega}_1 = \bar{x}_1 \omega_x + \bar{y}_1 \omega_y + \bar{z}_1 \omega_z \tag{14}$$

where

$$\begin{bmatrix} \omega_{1x} \\ \omega_{1y} \\ \omega_{1z} \end{bmatrix} = \begin{bmatrix} -1 & 0 & -\sin \phi_y \\ 0 & -\cos(\phi_x + \theta_1), & \cos \phi_y \sin(\phi_x + \theta_1) \\ 0 & -\sin(\phi_x + \theta_1), & -\cos \phi_y \cos(\phi_x + \theta_1) \end{bmatrix} \begin{bmatrix} \dot{\phi}_x \\ \dot{\phi}_y \\ \dot{\phi}_z \end{bmatrix} - \begin{bmatrix} \dot{\theta}_1 \\ 0 \\ 0 \end{bmatrix} \tag{15}$$

The small-angle assumption reduces the expressions to

$$\begin{aligned} \omega_{1x} &= -\dot{\phi}_x - \dot{\phi}_z \phi_y - \dot{\theta}_1 \\ \omega_{1y} &= -\dot{\phi}_y + \dot{\phi}_z (\phi_x + \theta_1) \\ \omega_{1z} &= -\dot{\phi}_z - \dot{\phi}_y (\phi_x + \theta_1) \end{aligned} \tag{16}$$

The inner gimbal angular velocity, $\bar{\omega}_2$, referred to inertial space, is that of the outer gimbal relative to space less that of the inner gimbal with respect to the outer gimbal.

$$\bar{\omega}_2 = \bar{\omega}_1 - \bar{x}_2 \dot{\theta}_2 \tag{17}$$

A transformation process similar to the one above yields

$$\bar{\omega}_2 = \bar{x}_2 \omega_x + \bar{y}_2 \omega_y + \bar{z}_2 \omega_z \tag{18}$$

where

$$\begin{bmatrix} \omega_{2x} \\ \omega_{2y} \\ \omega_{2z} \end{bmatrix} = \begin{bmatrix} -\cos\theta_2, & \sin(\phi_x + \theta_1)\sin\theta_2 & \sin\phi_y \cos\theta_2 + \cos\phi_y \cos(\phi_x + \theta_1)\sin\theta_2 \\ 0 & -\cos(\phi_x + \theta_1), & \cos\phi_y \sin(\phi_x + \theta_1) \\ \sin\theta_2, & -\sin(\phi_x + \theta_1)\cos\theta_2, & \sin\phi_y \sin\theta_2 - \cos\phi_y \cos(\phi_x + \theta_1)\cos\theta_2 \end{bmatrix} \begin{bmatrix} \dot{\phi}_x \\ \dot{\phi}_y \\ \dot{\phi}_z \end{bmatrix}$$

$$- \begin{bmatrix} \cos\theta_2 & 0 & 0 \\ 0 & 1 & 0 \\ -\sin\theta_2 & 0 & 0 \end{bmatrix} \begin{bmatrix} \dot{\theta}_1 \\ \dot{\theta}_2 \\ 0 \end{bmatrix} \tag{19}$$

For small angles,

$$\begin{aligned} \omega_{2x} &= -\dot{\phi}_x - \dot{\phi}_z \left(\phi_y + \theta_2\right) - \dot{\theta}_1 \\ \omega_{2y} &= -\dot{\phi}_y + \dot{\phi}_z \left(\phi_x + \theta_1\right) - \dot{\theta}_2 \\ \omega_{2z} &= -\dot{\phi}_z - \dot{\phi}_y \left(\phi_x + \theta_1\right) + \left(\dot{\phi}_x + \dot{\theta}_1\right) \theta_2 \end{aligned} \tag{20}$$

The above relationships can now be applied to Eq. (2) to derive the transfer functions of gyroscopic instruments used for angular measurements.

a. Two-Degree-of-Freedom (TDOF) Gyros

Applying Eq. (2) to the inner gimbal axis,

$$\left(\dot{\bar{H}}_2\right)_I = \left(\dot{\bar{H}}_2\right)_2 + \left[\left(\bar{\omega}_2\right)_I \times \bar{H}_2\right] = \bar{T}_2 \tag{21}$$

where $\bar{H}_2$ represents the total angular momentum of the gimbal and rotor.

$$\bar{H}_2 = \bar{x}_2 \omega_x I_{2x} + \bar{y}_2 \omega_y I_{2y} + \bar{z}_2 \omega_z I_{2z} + \bar{z}_2 H_r \tag{22}$$

where H_r is the angular momentum of the rotor (assumed constant)

x_2, y_2, z_2 are the principal axes of the inertia triad

I_2 are the corresponding principal moments of inertia.

If we assume that ω_{2z} is negligible with respect to H_r and that only those second-order terms multiplied by H_r are retained, appropriate substitutions will give the y_2 component of torque as

$$T_{2y} = H_r\left[\dot{\phi}_x + \dot{\theta}_1 + \left(\phi_y + \theta_2\right)\dot{\phi}_z\right] - I_{2y}\left(\ddot{\phi}_y + \ddot{\theta}_2\right) \tag{23}$$

This torque component can be equated to

$$D_2\,\dot{\theta}_2 + K_2\,\theta_2 + T'_{2m} \tag{24}$$

where D_2 = an inner gimbal viscous damping factor

K_2 = an inner gimbal spring rate

T'_{2m} = miscellaneous error torques and applied control torques

Including the ϕ_z term with the other error torques to form T_{2m}, we have, in Laplace notation,

$$\left(I_{2y}s^2 + D_2 s + K_2\right)\theta_2 - H_r s\theta_1 = H_r s\phi_x - I_2 s^2\phi_y - T_{2m} \tag{25}$$

representing the inner-gimbal axis equation in terms of the pickoff angles, θ_1 and θ_2.

Applying Eq. (2) to the outer-inner gimbal combination yields

$$\left(\dot{\bar{H}}_1\right)_I + \left(\dot{\bar{H}}_2\right)_I = \left(\dot{\bar{H}}_1\right)_1 + \left(\dot{\bar{H}}_2\right)_2 + \left[\left(\bar{\omega}_1\right)_I \times \left(\bar{H}_1 + \bar{H}_2\right)\right] = \bar{T}_1 \tag{26}$$

Expanding this expression as before to obtain the x_1 torque component, the outer-gimbal axis equation, in terms of the same pickoff angles, θ_1 and θ_2, is given by

$$\left[\left(I_{1x} + I_{2x}\right)s^2 + D_1 s + K_1\right]\theta_1 + H_r s\theta_2$$

$$= -H_r s\phi_y - \left(I_{1x} + I_{2x}\right)s^2\phi_x - T_{1m} \tag{27}$$

The solution to the pair of simultaneous equations, (25) and (27), after some rearranging, results in

$$\theta_1 = \left[\frac{A\left(D_1 s + K_1\right)}{H_r^2 s^2 + AB} - 1\right]\phi_x - \frac{H_r s\left(D_2 s + K_2\right)\phi_y - AT_{1m} - H_r s T_{2m}}{H_r^2 s^2 + AB} \tag{28}$$

and

$$\theta_2 = \left[\frac{B\left(D_2 s + K_2\right)}{H_r^2 s^2 + AB} - 1\right]\phi_y + \frac{H_r s\left(D_1 s + K_1\right)\phi_x - BT_{2m} - H_r s T_{1m}}{H_r^2 s^2 + AB} \tag{29}$$

where

$$A = I_{2y} s^2 + D_2 s + K_2$$

$$B = \left(I_{1x} + I_{2x}\right) s^2 + D_1 s + K_1$$

If we retain only the terms multiplied by H_r and neglect the damping factors and spring rates with respect to H_r,

$$\theta_1 \simeq -\phi_x + \frac{T_{2m}}{H_r s} \tag{30}$$

$$\theta_2 \simeq -\phi_y - \frac{T_{1m}}{H_r s} \tag{31}$$

Thus the pickoff angles are nearly proportional to the actual motion of the platform.

The two-gimbal system in an environment that permits unlimited vehicle rotation can induce a singularity referred to as "gimbal lock." Consider the relative gimbal orientation of the system shown in Fig. 2. A single possible 90° rotation of the platform (vehicle) about the y axis will align the x_p axis along the negative z_2 axis. A roll motion about x_p at this point would consist of a rotation about the spin axis. Used in a control system, the resulting false signal would result in a singularity in the stabilization system. Inserting the square matrix of Eq. (11) and solving $\dot{\phi} = f(\omega_p)$ show that the equations themselves forecast the difficulty for, as $\phi_y \to \pi/2$ radians, $\dot{\phi}_x$ and $\dot{\phi}_z$ approach infinity.

Thus a 90° displacement of the inner gimbal with respect to the outer gimbal causes "gimbal lock." In practice, the rotation of the inner gimbal is usually restricted to < 90° and the gimbal is assigned measurement of motions least likely to exceed that value. A better solution for missions calling for larger angular rotations is to bypass the two-gimbal system in favor of a three- or four-gimbal system.

b. Single-Degree-of-Freedom (SDOF) Gyros

Fig. 3 is a schematic of a single-degree-of-freedom (SDOF) gyro mounted on a single-axis platform. We retain four descriptive coordinate systems as before, but redefine the axes in each system.

SDOF

1. Inertial space (x_I, y_I, z_I)
2. Vehicle (x_v, y_v, z_v)
3. Platform (x_p, y_p, z_p)
4. Gimbal (x, y, z)

TDOF (Previously Defined)

1. Inertial space (x_I, y_I, z_I)
2. Platform (x_p, y_p, z_p)
3. Outer Gimbal (x_1, y_1, z_1)
4. Inner Gimbal (x_2, y_2, z_2)

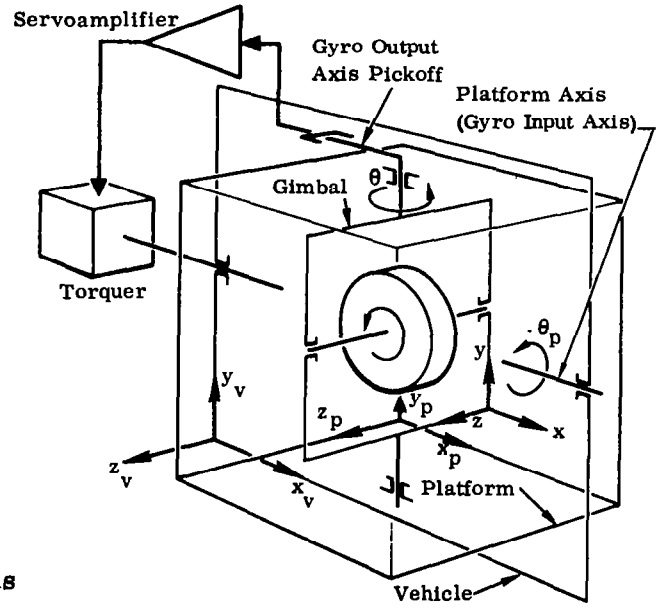

Figure 3. Schematic of SDOF Gyro on Single-Axis Platform

Since the resolution of the systems of axes is identical to that performed earlier, the input-axis equation can be obtained directly from Eq. (27) with appropriate substitution of subscripts. Neglecting the D_p and K_p terms with respect to the platform inertia reaction torque, we can write:

$$\theta_p + \phi_x = \frac{-H_r s\left(\theta + \phi_y\right) - T_{pm}}{\left(I_x + I_{px}\right) s^2} \tag{32}$$

Similarly, the gimbal pickoff angle, θ, or the output-axis equation is obtained from Eq. (25):

$$\theta = \frac{H_r s\left(\phi_x + \theta_p\right) - I_y s^2 \phi_y - T_m}{I_y s^2 + Ds + K} \tag{33}$$

In terms of the axis under consideration, the $I_y s^2 \phi_y$ input may be considered an error torque and lumped with T_m. The gyro output measurement is then approximated by

$$\theta = \frac{H_r s\left(\phi_x + \theta_p\right) - T_m}{I_y s^2 + Ds + K} \tag{34}$$

where $s(\phi_x + \theta_p)$ represents the input rate, $\omega_i(s)$, of the platform on which the gyro is mounted.

Several classes of gyroscopes constrained to one degree of freedom are represented by this transfer function through the control of its characteristic parameters.

3.1.1.1 Gyroscope Types

Rate Gyros. A known spring restraint can be added, to increase the value of K such that θ becomes nearly proportional to $d(\phi_x + \theta_p)dt$, thus making the instrument a rate-measuring device.

Assuming no error or control torques ($T_m = 0$), Eq. (34) can be written as

$$\frac{\theta}{\omega_i}(s) = \frac{H_r/K}{\left(I_y/K\right)s^2 + (D/K)s + 1} \tag{35}$$

The steady-state response to (35) is given by

$$\theta(s) = \frac{H_r}{K}\,\omega_i(s)$$

or

$$\theta \propto \omega_i$$

which shows that if the input to a rate gyroscope is an angular velocity, ω_i, the output is an angle, θ, that is proportional to ω_i.

The choice of K is influenced to some extent by the rapid damping requirements, which necessitate high D/I_y ratios. Because of the desired proportionality, K must be tailored such that D/I_y can be neglected with respect to K/I_y. Hence the natural frequency of a rate gyro (generally > 15 cps), tends to be on the high side with respect to some of the frequencies (rigid body, first few bending and sloshing modes) affecting the stability and control loops of launch vehicles.

Rate gyros are readily available to measure maximum rates from less than 10 to more than 100 deg/sec with resolutions ranging from 10:1 to as high as 5000:1 in some miniature components. Good subminiature fluid-filled units weighing less than 4 ounces are also available with maximum rates of 15 to 1000 deg/sec and resolutions better than 200:1.

Rate-Integrating (Displacement) Gyros. The theory of operation of a rate-integrating (displacement) gyro is similar to that of a rate gyro. The basic difference is that in the latter, the damping restraint is kept as low as possible while meeting the damping requirements, whereas in the former, the spring restraint is kept as small as possible. The result is that Ds in Eq. (34) becomes the dominant factor in the characteristic equation and θ is nearly proportional to $(\phi_x + \theta_p)$.

In (34), let K = 0 and neglect T_m. After some rearranging, we can write

$$\frac{s\theta}{\omega_i}(s) = \frac{H_r/D}{\left(I_y/D\right)s + 1} \tag{36}$$

which has a steady-state response

$$\frac{s\theta}{\omega_i}(s) = \frac{H_r}{D}$$

or

$$\theta \propto \int \omega_i \, dt$$

Since $\int \omega_i \, dt$ represents a total angle, the precession (output) angle, θ, is proportional to the total input displacement angle.

The dynamic response of such a gyro in the frequency range of interest can therefore be adequately represented by a first-order lag with a time constant (characteristic) of I_y/D, which is usually measured in milliseconds.

These gyros are always used in null-seeking servo loops whose error signal is provided by the gyro precession axis output. Thus very little angular motion need take place about this axis; this is usually limited to ±2°. In a "strap-down" application, the slower vehicle response when compared with that of a gimbaled platform leads to larger gimbal errors before flight corrections can be made. "Wide angle" gyros with gimbal freedom of ±10° or more have been developed and are used for this purpose.

Integrating Gyros. If both the spring and damping restraints are kept small with respect to the rotor inertia, θ becomes proportional to $\int(\phi_x + \theta_p)dt$, producing an "integrating gyro."

Let $K = D \simeq 0$ in Eq. (34) and neglect T_m as before. The resulting expression can be written

$$\frac{s\theta}{\omega_i}(s) = \frac{H_r}{I_y} \tag{37}$$

Manipulation of (37) will show that

$$\theta \propto \int (\text{Total angular displacement input})\, dt$$

In practice, some small damping is provided by the viscosity of the fluid in which the gimbal is floated, whereas the spring restraint is almost entirely eliminated. A better representation, therefore, is that of a first-order lag with a high time constant.

Gyros of this type are capable of very high accuracy and are usually employed in conjunction with platforms in inertial-navigation systems.

Neglecting the spring and damping restraints in Eqs. (32) and (33) and eliminating θ yields an expression for the input $(\phi_x + \theta_p)$ with a characteristic equation

$$\left(I_x + I_{px}\right)s^2 + H_r{}^2/I_y$$

The roots of this equation, $\pm j\, H_r / \sqrt{I_y (I_x + I_{px})}$, represent the frequency at which the undamped gyro platform tends to oscillate; i.e., its natural resonant or "nutation" frequency.

3.1.1.2 Displacement Gyros

The primary function of a displacement gyro is to provide an accurate angular reference. On a vehicle, three such references are required to establish an attitude reference triad associated with the vehicle pitch, yaw, and roll axes. Inputs to the reference axes of body-mounted gyros include vehicle angular motion and signals to the torquers from open-loop steering programs and closed-loop guidance.

This angular reference can be obtained from many sources, such as SDOF gyros, TDOF gyros (two required), inertial platforms (particularly if inertial guidance is contemplated), and noninertial-type sources (optical, radar, etc.). In general, consideration of the missions and the guidance required dictates the type of sensors to be used, although the weight, power requirements, and reliability of present-day noninertial instruments place them at a disadvantage. The TDOF gyro has several minor disadvantages when its construction is considered. Excursions off-null are more limited than for the SDOF gyro. Methods of torquing also present difficulties. Although TDOF gyros compete with SDOF gyros for platform and aircraft applications, where acceleration levels are lower, they do not appear to compete favorably for strapped-down applications in launch vehicle environments.

As a primary attitude sensor, therefore, a system of SDOF, floated, rate-integrating gyros mounted in such a manner as to assure orthogonality has many advantages:

a. No preflight package alignment is required other than at the time of installation, and no additional computations are required. The gyros, however, must be caged until just prior to launch.

b. Relatively accurate open-loop maneuvers can be performed without guidance sensing, commands, or computations.

c. When closed-loop guidance is carried out, the contribution of the attitude reference drift to guidance errors is acceptably small.

The disadvantages of such a system for use with a guidance system employing a continuous attitude reference are:

a. The control system gyros are series-dependent, thereby degrading reliability.

b. The drifts of the gyros, although small, represent additional sources of error in the system.

From a functional standpoint, a gyro consists of its basic mechanical components and electrical accessories (pickoff, amplifiers, torquer, etc.). Thus transfer

functions can be written for gyro output-to-inertial input and for gyro output-to-torquer input. The units of the transfer function depend on the implementation of the signal-pickoff/signal-amplifier combination and the torquer/torquer-amplifier combination. Data may be analog or digitally encoded at the input and output.

The signal pickoff is operated in a null-seeking servo loop. High sensitivity and low drift (or null shift) are the dominant requirements, while constancy of scale factor is subordinate. Either analog or digital (pulse) encoding of pickoff information can easily satisfy these requirements. Therefore, the method of encoding may be chosen to simplify mechanization of the remaining portions of the flight control system, thus enhancing reliability. Conversely, torquers or torque motors have severe scale factor constancy requirements if open-loop maneuvers are to be performed by applying preset torque-time histories. Consequently, the implementation (should one implementation offer significant accuracy improvement over the other) should be selected to meet the accuracy requirements.

a. Analog-Torqued Gyros

Fig. 4 shows a typical application of an analog-torqued gyro in a launch vehicle control system. The gyro senses the angular rate of the vehicle turning about its input axis and precesses about its output axis through an angle proportional to the time integral of the input axis rate. The gyro signal generator produces a signal proportional to this displacement, and this signal, properly shaped and with appropriate gain, is used to deflect the control vector, creating a vehicle rate about the gyro input axis in the proper direction to null the gyro output displacement. (The vehicle is thus made to follow a trajectory with an inertially fixed attitude.)

To alter vehicle attitude, the gyro torquer applies a torque about the output axis of the gyro. This torque causes an angular deflection of the gyro about the output axis similar to that caused by an input axis rate. The vehicle is thus commanded to turn at a rate sufficient to drive the output axis deflection to zero. Upon removal of the output axis torque, the vehicle again assumes an inertially fixed attitude rotated through an angle proportional to the time integral of the applied torque. Since the torquer amplifier is continuously connected to the torquer, any noise or null error (offset) in the torquer amplifier causes a torque input to the gyro and consequently a time-integral error in the gyro displacement. Similarly, any scale factor shift or gain drift in the amplifier causes an accumulating error proportional to the commanded attitude change.

Functional Requirements. Gyro functional requirements should be made up of all items that can affect launch vehicle stability and control, from the mounting of the instruments to the torquer input characteristics. Other requirements, primarily

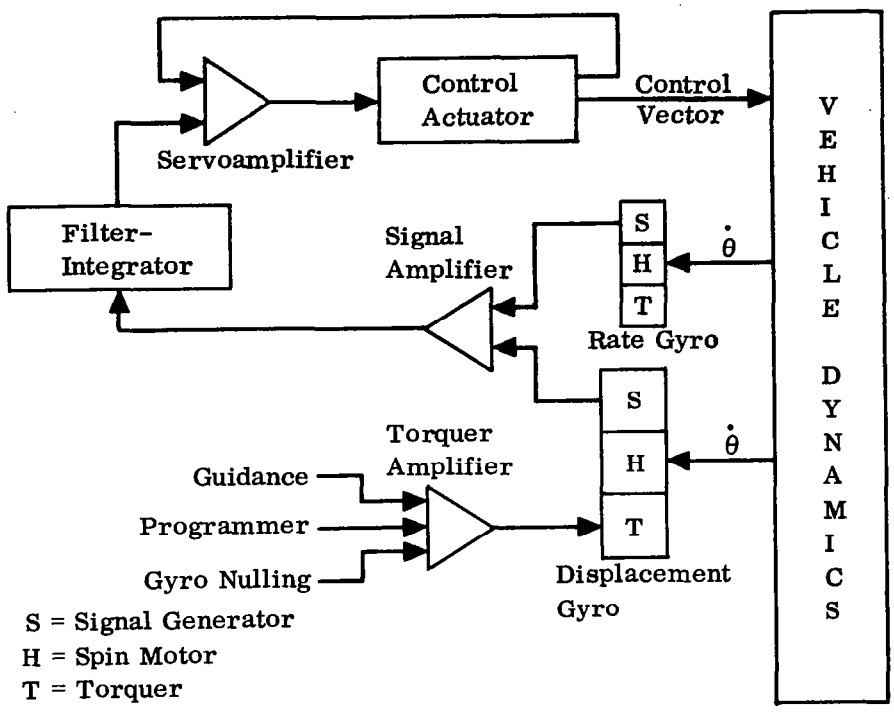

Figure 4. Typical System Using an Analog-Torqued Gyro

concerned with guidance compatibility, environmental loads, thermodynamics, etc., do not form part of this discussion.

The mounting (packaging) of displacement gyros should be such as to minimize local elastic deflections. Further, their "placement" or allowable positioning should be restricted. If vehicles were completely rigid, displacement gyros could be positioned anywhere on the launch vehicle (longitudinally and laterally). However, vehicles are not rigid, and elastic deformations (bending) do exist. These elastic deformations are sensed by the gyros in the same manner as rigid-body attitude errors are sensed, and the resultant gyro output consists of the superposition of these signals. Restricting the gyro placement to those portions of a launch vehicle where the elastic deformations (especially of the lower elastic modes) are small results in spurious oscillation amplitudes usually below the response threshold of the engine-actuator system.

The pitch and yaw first modal deflections are generally largest at the extreme ends of a vehicle; thus these locations should be avoided for pitch and yaw displacement gyro positioning. Midbody positions present better alternatives. Interstage adapter areas are also worth considering in configurations employing relatively long upper stages; e.g., the Atlas-Agena combination. Torsional frequencies tend to be

widely separated from the control frequency, so that roll gyro placement is satisfied on a firm structural mount that is relatively free from local deformations. The extreme ends of a vehicle, where torsional deflections are greatest (for first torsional mode) should be avoided.

Ideally, the gyro input axes form an orthogonal triad congruous with a defined autopilot reference triad. The error in gyro alignment has two sources: the nonorthogonality of the three gyro input axes determined by the gyro mounting within the gyro package; and the noncongruity of the gyro package with the autopilot reference axes determined by the gyro package mounting on the structure. The primary effect of gyro misalignment on stability is the introduction of crosscoupling between control channels. This crosscoupling should be looked into, although its effect can be shown to be negligible on some vehicles. This is demonstrated in the following brief analysis carried out for an existing liquid propellant vehicle.

Assume a control system with coupling between pitch and yaw due to a misalignment (noncongruity) of the gyro package by angle ϵ about the roll axis. Fig. 5 is a simplified block diagram of the pitch and yaw channels of a control system, including the noncongruity crosscoupling terms. The small-angle approximations, $\sin \epsilon \simeq \epsilon$, $\cos \epsilon \simeq 1$, and $\epsilon^2 \simeq 0$, have been assumed.

Fig. 6 shows typical root loci with $\epsilon = 0$ and $\epsilon = 10^\circ$. The original locus divides into two loci, which, for small ϵ, are extremely close to the original. As can be concluded from the figures, misalignment of less than 10° is tolerable, 5° acceptable, and 1° negligible from the standpoints of stability and control. A similar effect is obtained for yaw and roll.

In the case of gyro-to-package misalignment (nonorthogonality), one of the crosscoupling terms in Fig. 5 is zero while the other is not. Therefore, only one channel would exhibit the split loci. The effect on stability is identical.

A displacement gyro is subject to, and must respond to, angular accelerations and rates stemming from various torques applied to the vehicle. A displacement limit should therefore be stipulated as a maximum excursion, about the input axis, that does not cause the gyro to reach its mechanical limits about the output axis. These limits should be set from consideration of all intended applications of the launch vehicle with regard to: the steady-state "bucking" of commanded body rates; anticipated flight transients and oscillatory demands from winds, gusts, staging, etc.; steering or guidance requirements; and compatibility with control capability during periods of greatest potential demands.

Fig. 7 presents the results of a survey of a number of light-payload missiles to determine the demands placed on the displacement gyros in flight. The magnitude of the displacement gyro excursions was obtained from telemetry

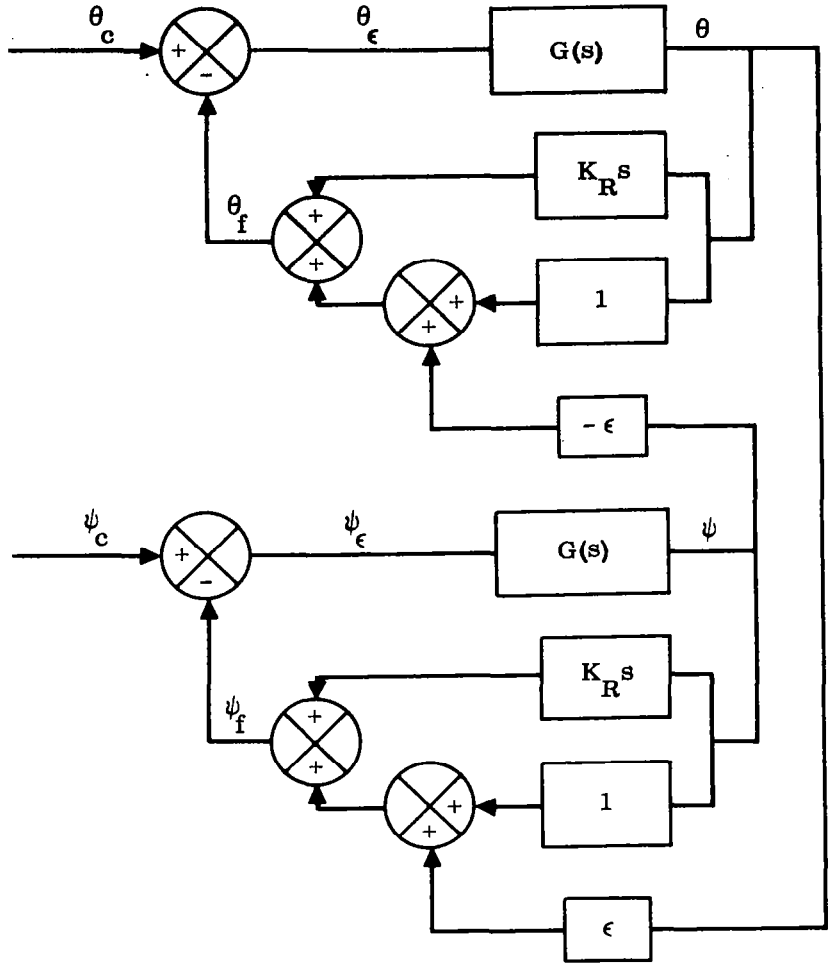

Figure 5. Control System Block Diagram, Including Displacement Gyro Noncongruity

records of 51 flight articles. (The number of entries exceeds the sample size since there were several entries per sample.) These data do not include the roll program displacement, since this is highly mission-dependent.

With a rate-integrating gyro used as an attitude reference instrument, the allowable linearity error can be quoted in percentage deviation from the nominal straight-line fit (passing through the origin) of the gyro gain data. The threshold is that level below which the output will not be expected to track the input. However, the output will be expected to stay below the value associated with the threshold as long as the input is below this value. Specifying threshold is necessary, since the percentage deviation for linearity cannot be carried to zero input. These data should be measured at frequencies low enough to avoid dynamic effects. Fig. 8 shows this characteristic.

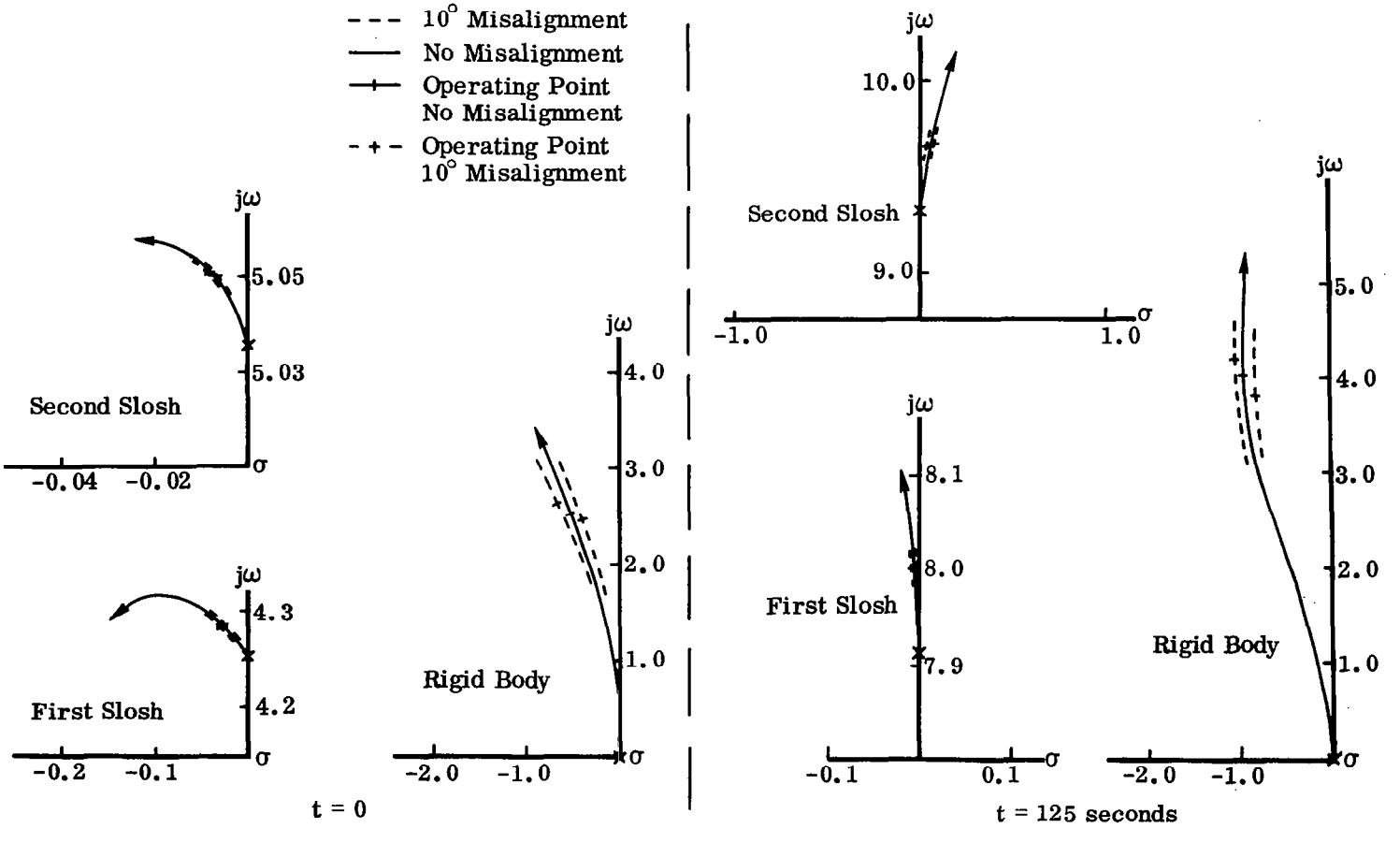

Figure 6. Typical Root Loci Showing Effect of Pitch and Yaw Coupling Due to Noncongruity (Displacement Gyro)

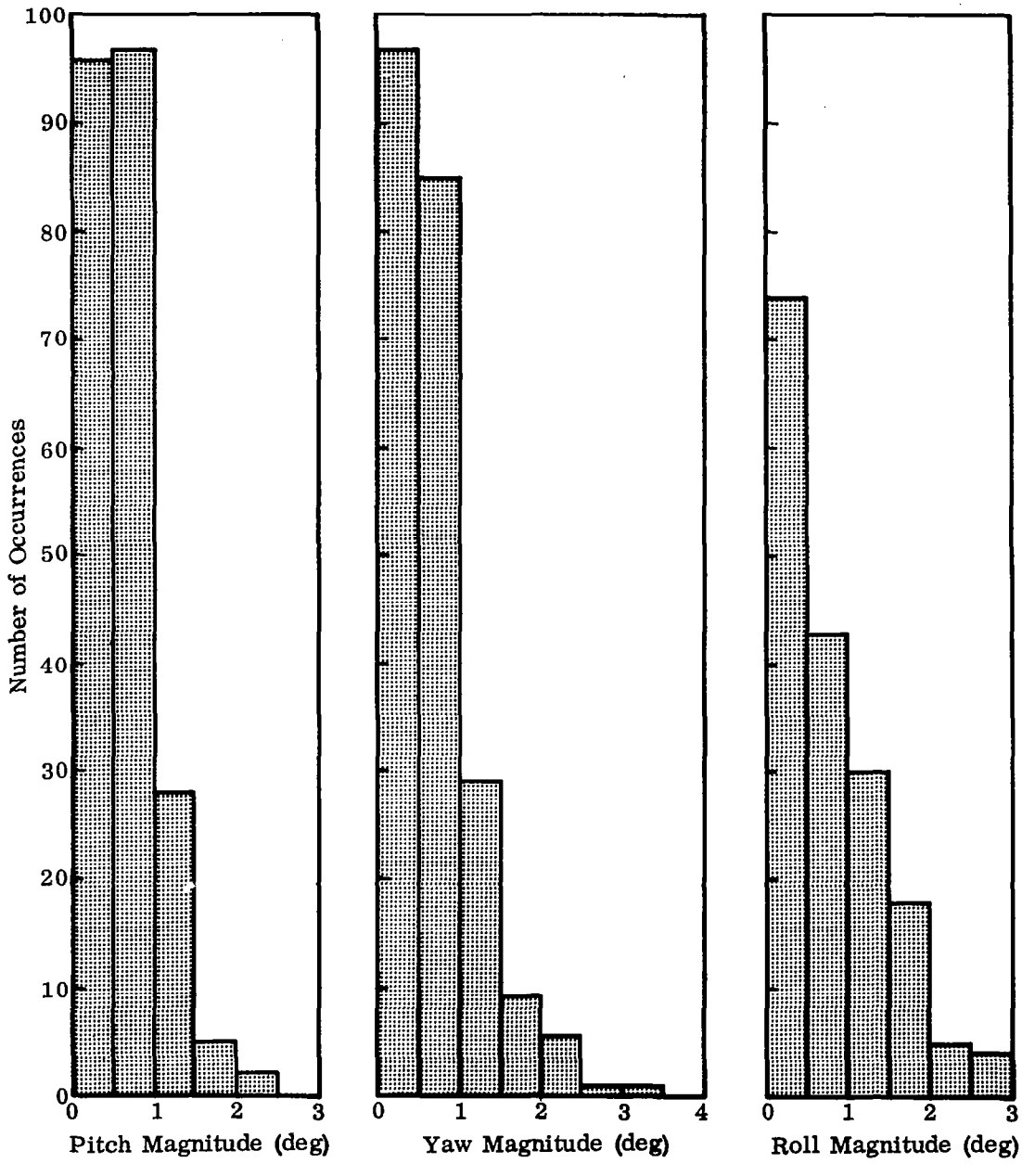

Figure 7. Maximum Excursion Histograms, Displacement Gyro

This approximation may not be completely adequate. For extremely small input angular rates, the precession torque is extremely small, usually smaller than the static friction in the gimbal support bearings. Thus there is no motion about the output axis in response to this input angular rate. The usual term applied to this is "stiction," and typically the stiction rate is $< 10^{\circ}/hr$. For rates above that required to overcome the stiction, there is some bearing friction torque that is even smaller (gyro drift).

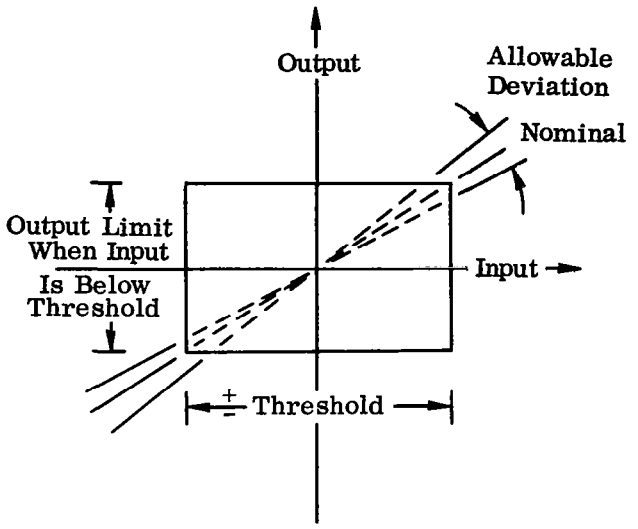

Figure 8. Output Linearity and Threshold Approximations for Rate-Integrating Gyros

Stiction can be ignored if it is assumed that the input angular rate to the gyro is in excess of the stiction rate at all times during flight. This should be a valid assumption, in that a stiction rate of $0.003^{\circ}/sec$ should be well below the threshold of most flight control system channels. Since the gyro is subjected to the small limit cycle (around this threshold amplitude) usually present on a launch vehicle, input rates will be higher than stiction rates, and the approximation of Fig. 8 becomes valid throughout the flight mode.

Gyros should be linear within their expected range of inputs, allowing for the full travel required of the control system. Threshold limits for stability and control applications depend on, and should be set below, the threshold capability of the control-actuation system. Limits $\leq 0.02^{\circ}$ are well within the state of the art.

Having the highest frequencies of concern (~ 40 radians in bending and sloshing) remain somewhat below the gyro corner frequency allows transfer function representation by a constant gain factor in all but the most critical analyses. Further, constancy of transfer function during flight is highly desirable, to avoid variations in the compensation required. This applies particularly in the pitch and yaw axes. In roll, the rigid body control mode (frequency range $0 \sim 2.5$ cps) is the only mode of concern, because the parasitic modal frequencies (torsional modes) are usually on the order of 12 cps or higher. Therefore, it is not necessary to require a flat response over a large frequency range when the roll displacement gyro is used in conjunction with a roll rate gyro, although such a response is satisfactory. The frequency at which the response deviates from "flat" merely affects the electronic compensation (lag filtering) required to "roll off" the system

response. With a lead filter (derived rate) network replacing the roll rate gyro, the lead filter circuitry requires additional "poles" (or lags) to obtain the required signal shaping for noise suppression as well as for system stability. As such, the system becomes more sensitive to phase uncertainties at lower frequencies. For some applications, it should be required that the roll displacement gyro response be flat over a large frequency range to minimize gain and phase uncertainties at the lower frequencies.

Gyro nulling, steering programs, and guidance commands are generally introduced to the closed-loop control system via torquer command inputs. Steering introduced as a series of rate levels to the torquer (see Fig. 9) presents no difficulties, providing the levels are of small amplitude and sufficient time is allowed between the levels. Guidance commands through a decoder may appear as a series of steps, each of small duration t. A simple lag inserted between the guidance decoder and the torquer amplifier will serve to avoid a forced oscillation at the (1/t) cps frequency.

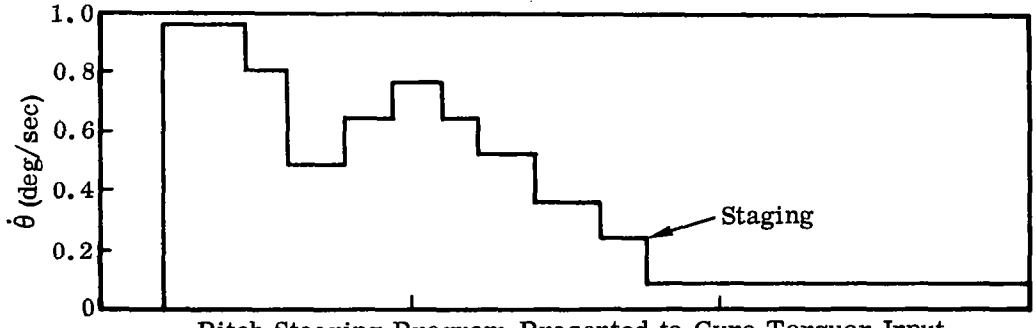

Pitch Steering Program Presented to Gyro Torquer Input

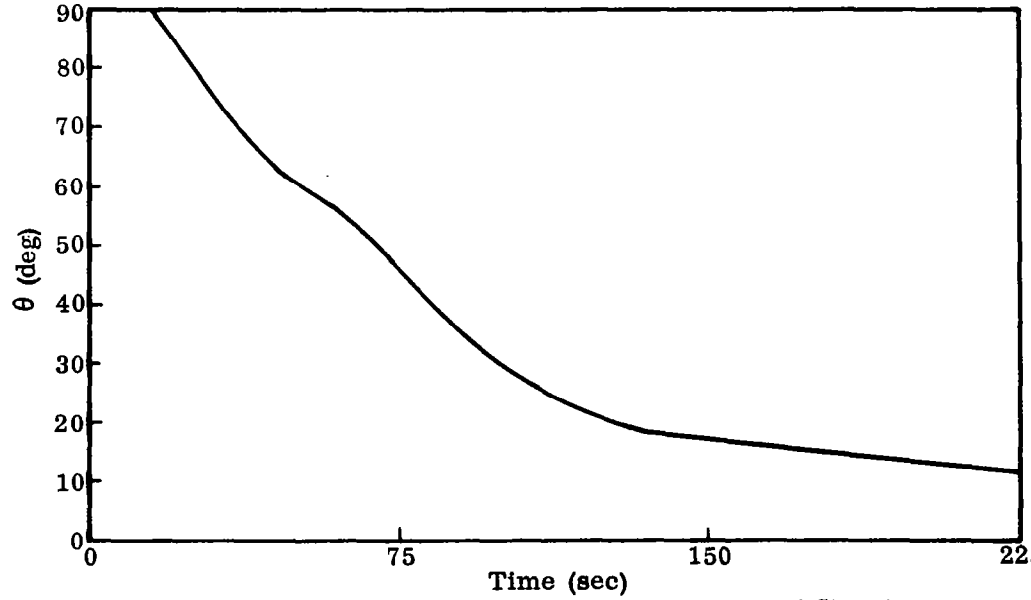

Angular Displacement History Caused by Analog-Torqued Steering Program

Figure 9. Typical Analog-Torqued Pitch Steering Program and Angular Displacement History

Transfer Function. Fig. 10 is a typical block diagram for an SDOF rate-integrating gyro. The input signal sources are: the vehicle rate of motion, ω_i; and the commands, E_i (from steering or guidance), to the torquer.

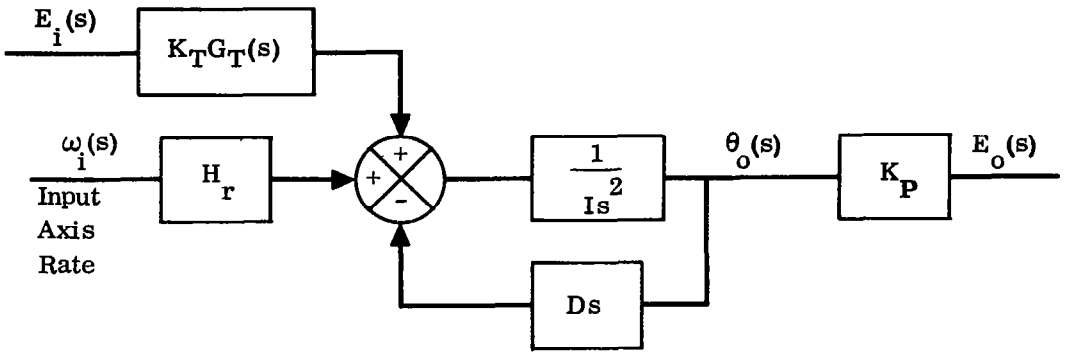

Figure 10. Block Diagram of Rate Integrating Gyro

The transfer function is obtained from Eq. (36), where

$$K = 0 \quad \text{(rate integrating gyro)}$$

$$s\left(\phi_x + \theta_p\right) = \omega_i(s)$$

$$-T_m = E_i K_T G_T(s)$$

where $K_T G_T(s)$ is the torquer transfer function

giving

$$\theta_o(s) = \frac{H_r \omega_i + E_i K_T G_T(s)}{Is^2 + D s} \tag{38}$$

Then the respective transfer functions are:

Command Torques

$$\frac{E_o}{E_i}(s) = \frac{1}{s} \frac{\frac{K_P K_T}{D} G_T(s)}{\frac{I}{D}s + 1} \tag{39}$$

Input Axis Rates

$$\frac{E_o}{\omega_i}(s) = \frac{1}{s} \frac{\frac{K_P H_r}{D}}{\frac{I}{D}s + 1} \tag{40}$$

where $E_o = K_P \theta_o$.

The total transfer function is:

$$E_o = \frac{1}{s} \frac{\frac{K_P}{D}}{\left(\frac{I}{D}\right)s + 1} \left[H_r \omega_i + E_i K_T G_T(s) \right] \tag{41}$$

If we assume that I/D is very small and that the gyro can be represented by some gain factor, K_G, in a given frequency range, then the gyro-output/torquer-input transfer function can be given by

$$\frac{E_o}{E_i}(s) = \frac{K_G}{s\left(\tau_T s + 1\right)} \tag{42}$$

where τ_T is the torquer time constant ($\tau_T \leq 10$ milliseconds).

A similar approximation can be made for the gyro-output/input-rate transfer function.

It should be pointed out that tailoring or specifying the inputs to the torquer, rather than the torquer transfer function itself, is a common method of insuring the stability of a vehicle.

b. Pulse-Torqued Gyro

In a pulse-torqued displacement gyro system, calibrated pulses rather than amplitude-modulated signals are fed to the torquer. Accurate torquing requires pulses having fixed amplitude and duration. This replaces the linearity requirement of the analog system with one of constancy. These pulses displace the gyro angular reference attitude incrementally, assuming that the angular momentum of the gyro remains constant. This introduces "granularity" or quantization errors.

When employing fixed-amplitude and -duration pulses, the gyro reference attitude can assume only discrete attitudes separated by an incremental angle, $\Delta\theta$, represented by one pulse. Since the incremental angle is proportional to the amplitude and duration of the applied torque pulse and is inversely proportional to the gyro angular momentum, these may be adjusted to arrive at a specified granularity.

In order to rotate the gyro reference at some average angular rate (ω_{avg}), it is necessary to generate the pulses at some average rate, represented by the pulse repetition frequency (PRF), which is equal to $\frac{\omega_{avg}}{\Delta\theta}$ pulses per second or $\frac{\omega_{avg}}{\Delta\theta} \times T$ pulses per cycle, where T is the cycle time of the programmer or guidance system in seconds per cycle. For example, if

$$\Delta\theta = 0.01^\circ/\text{pulse}$$

$$\omega_{avg} = 10^\circ/\text{sec}$$

$$T = 1 \text{ sec/cycle}$$

then

$$PRF = 1000 \text{ pulses/cycle}$$

Using the same $\Delta\theta$ and T, the smallest nonzero ω_{avg} attainable is equivalent to a PRF of 1 pulse/cycle, or $\omega_{avg} = 0.01^\circ/\text{sec}$. This illustrates some other important specifications: minimum and maximum average torquing rates. These are used by the designer in specifying the cycle time and maximum PRF. Once the cycle time and PRF are arrived at, there are several ways to implement a programmer; e.g., a gated clock or a binary rate multiplier. These, however, fall outside the scope of this monograph and will not be treated here.

A pulse gyro may be operated directly with an analog signal autopilot. Fig. 11 shows that the torquer is not in the closed-loop portion of the autopilot but represents the external input to the system. Comparison with Fig. 4 shows that the closed-loop portion of the autopilot remains unchanged. Only the displacement gyro torquer and its input change from analog to digital (pulse) encoding. As long as the pulse repetition frequency (or a subharmonic of it) does not coincide with the launch vehicle modal frequencies, the stability of the closed loop will not be appreciably affected by the torquing pulses. An additional restriction must be placed on the pattern of pulses applied to the torquer by a programmer and/or guidance. Since this pattern is impressed on the attitude control system, forced oscillation is possible and should be analyzed carefully.

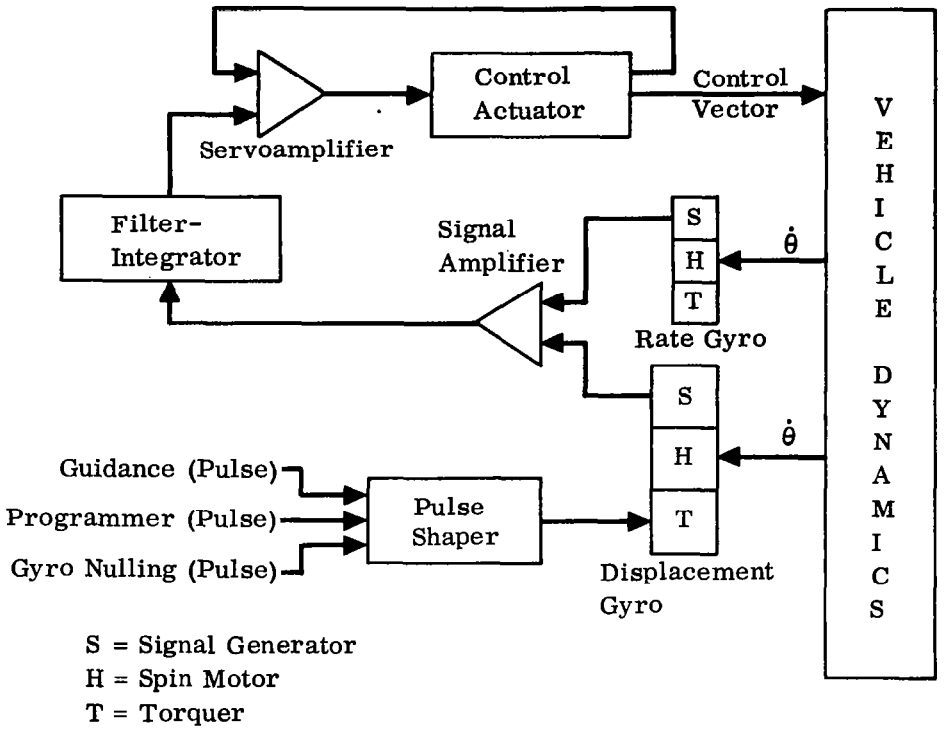

Figure 11. Typical System Using a Pulse-Torqued Gyro

Fig. 12 shows an alternate implementation whose dominant feature is the introduction of an additional feedback loop around the gyro. This loop keeps the gyro output axis near null and operates in the following manner.

Any deviation of the vehicle attitude from the gyro reference attitude is detected and amplified. If the resultant signal exceeds the threshold, a flip-flop is triggered, and a pulse of calibrated amplitude and duration is fed to the torquer to move the gyro through an angular increment, $\Delta\theta$. This same pulse is added to a reversible binary counter, converted to an analog signal, and used in the analog portion of the autopilot in a manner similar to the attitude error signal employed in the analog signal autopilot.

The advantage of such gyro rebalancing is that the gyro spin motor wheel remains near the null position at all times. This allows very small "expected angular excursions." Therefore, small size and/or more accurate compensation of g-sensitive or off-null-sensitive drift should be possible.

The requirements for a pulse-torqued gyro are the same as for an analog-torqued gyro with the exception of those applicable to the torquer.

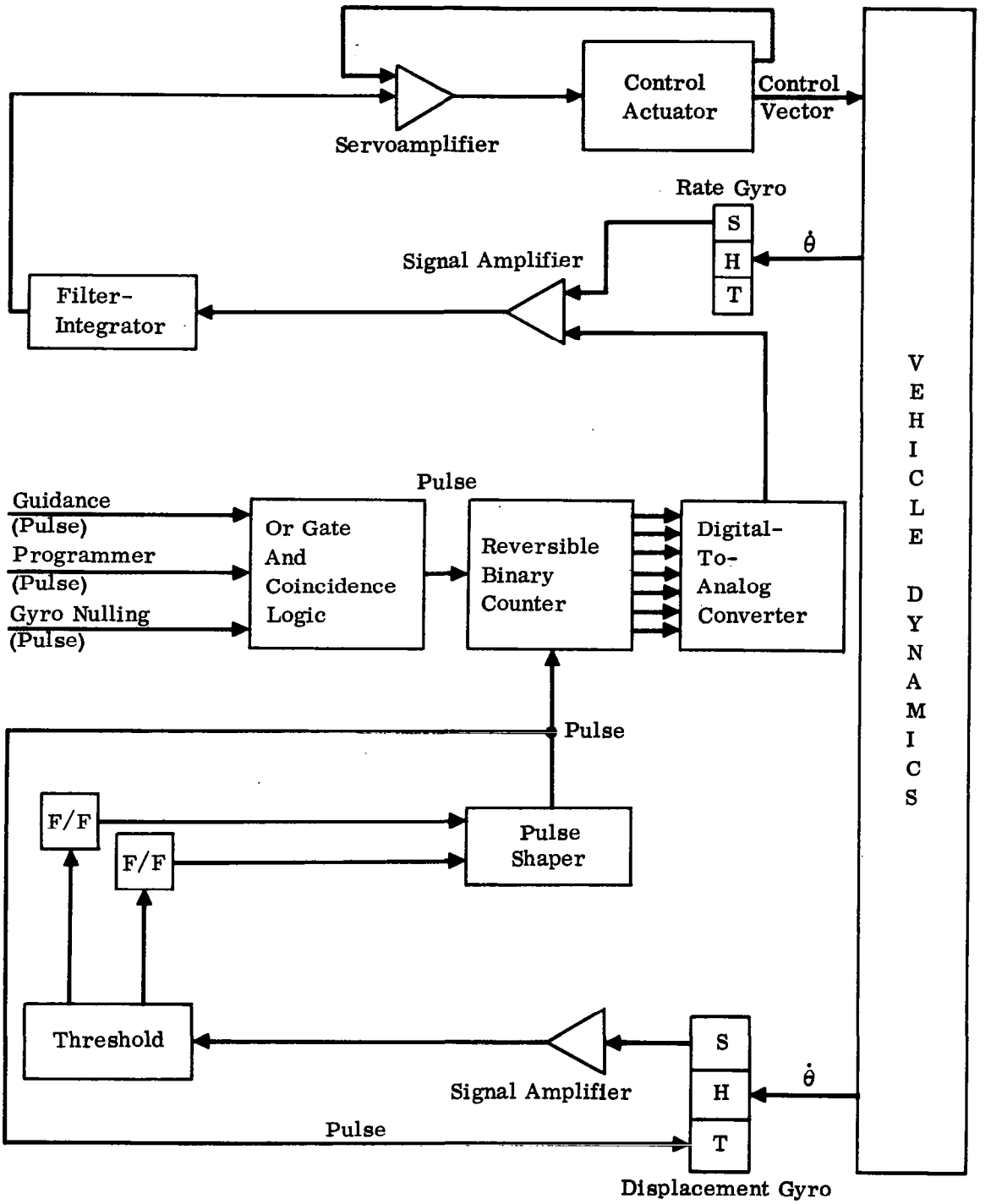

Figure 12. Functional Diagram of a Typical Control System Using a Pulse-Torqued Gyro with Pulse Rebalance Feedback

Care must be exercised in selecting a pulsing technique that minimizes the excitation to the control system. A good choice would be one that provides uniform spacing of pulses over the cycle period without degrading the accuracy of the gyro system. Stability constraints may have to be imposed on other system parameters, in lieu of conditioning this type of torquer input signals. The parameters referred to are: the minimum attainable rate level, ω_{min}; the maximum required rate level, ω_{max}; and the minimum allowable increment of displacement.

The minimum increment of gyro displacement is obviously equivalent to the pulse weight, $\Delta\theta°$/pulse, which is a function of pulse amplitude and duration. This establishes the "pointing" granularity and is important in obtaining accurate vehicle orientation. Guidance reorientation and a roll program that establishes launch azimuth are examples of maneuvers that depend on the specification of $\Delta\theta$. To preclude a forced oscillation, the pulse trains from the programmer and guidance system should be compatible. Large, low-frequency pulsing commands can degrade system stability margins and should be avoided. Keeping the pulse weight below the control-actuating system threshold provides another means of minimizing the incidence of forced oscillations.

The stability and response characteristics under the influence of the pulse-torquing commands depend enough on the particular application to require a complete analysis for each configuration.

3.1.1.3 Rate Gyros

A common method of stability compensation in launch vehicle attitude control systems is the introduction of rate information. The angular rate of motion of a vehicle may be measured directly from a gyroscopic device or indirectly from the integration of some acceleration signal as well as from the differentiation of a displacement measurement.

A rate gyro measures angular velocity by measuring the gyroscopic torque that accompanies, and is proportional to, this angular velocity. An angular rate about the input axis causes a precessional torque about the output axis, which is reacted upon by the torque of the spring restraint. In the steady state, the output axis angular deflection is then proportional to input axis angular rate. A signal pickoff encodes the angular deflection of the output axis.

In launch vehicle applications, the rate signals so generated are used in conjunction with an attitude reference instrument (e.g., displacement gyro) signals to provide the damping required to stabilize the control loop.

a. Functional Requirements

Since the primary function of rate gyros is stabilization, stability and control considerations dictate the basic requirements for rate information. Most other

requirements come in the form of constraints placed on the implementation of the rate gyro.

Rate gyros that are physically attached to a vehicle structure detect total case motion (or vehicle motion) with respect to inertial space. The gyro cannot distinguish between rigid-body motions (the motions actually being controlled) and those due to vehicle elastic deformations. These elastic deformations are generally significant in pitch and yaw. By placing the pitch and yaw rate gyros forward of the first mode antinode, this mode may be phase-stabilized during those portions of flight for which the first mode is not strictly gain-stable (disregarding phase). The gyros, however, should not be located so far forward as to sense large signals at the first mode frequency. The torsional mode excitation sensed by the roll rate gyro is usually small and of high enough frequency that any position that avoids local elastic slopes is satisfactory. The extreme ends of the vehicle, where torsional slopes are greatest (for first torsional mode), should be avoided.

Rate gyro alignment is made up of two components: orthogonality (gyro-to-package) alignment; and congruity (package-to-vehicle) alignment. The total gyro-to-vehicle alignment is a root-sum-square (RSS) value of the two misalignments. Proper manufacturing techniques can restrict the nonorthogonality to 0.3° or less. As a result, the congruity alignment assumes more importance.

As for the displacement gyros, the primary effect of misalignment on stability is crosscoupling between channels. Fig. 13 is a simplified block diagram of the pitch and yaw channels showing the crosscoupling terms due to a misalignment of the gyro package by the small angle, ϵ, about the roll axis. Fig. 14 shows the results of an analysis performed on an existing vehicle; the original locus divides into two loci.

In case of nonorthogonality, one of the terms of Fig. 13 is zero. Therefore, only one channel would exhibit the split loci.

Driving a rate gyro to its mechanical stop does not necessarily constitute a failure but is to be avoided where possible. A rate limit should therefore be stipulated for a maximum angular rate about the input axis that does not cause the gyro to reach its mechanical limits about the output axis. In establishing limits, the governing factor should be the flight transient and oscillatory rate demands arising out of the configuration requirements that react most strongly to environmental torques. Further, the roll requirements must consider the large liftoff transients that result from small differential offsets in booster engines yaw/roll alignments that remain uncorrected unless control is activated immedatiely at liftoff. The lower moment of inertia about the roll axis can give rise to increased roll rate requirements due to this cause alone.

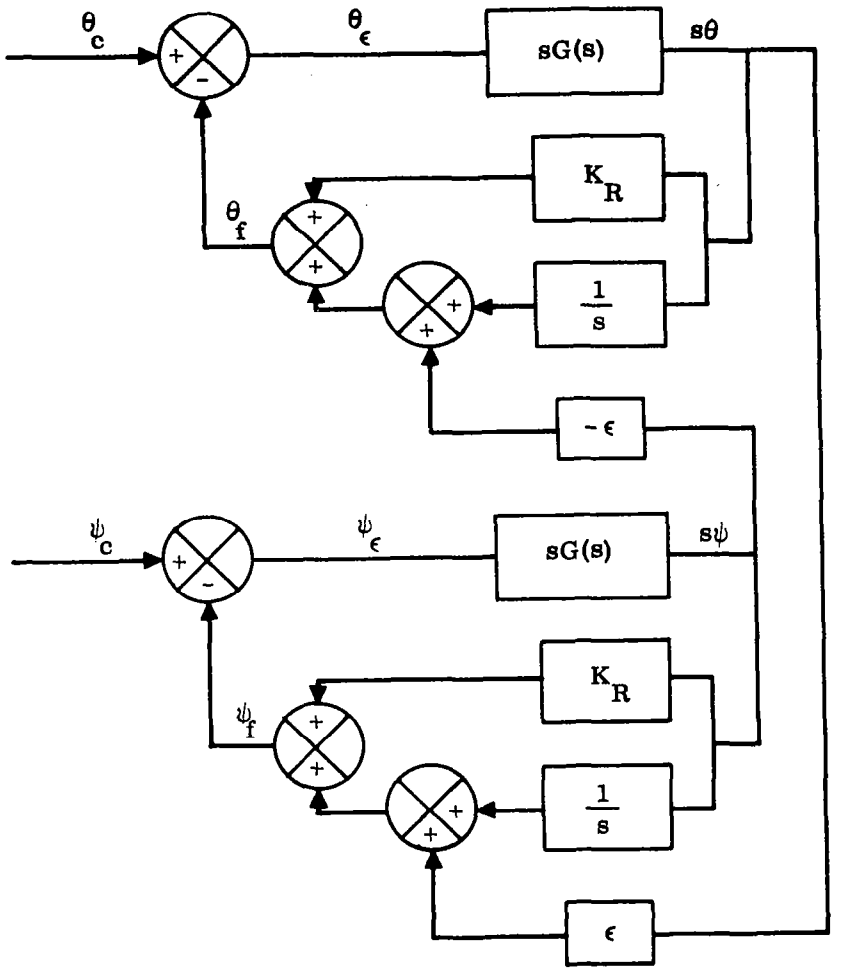

Figure 13. Control System Block Diagram, Including Rate Gyro Noncongruity

A survey was made of a number of payloads: very light (Nike-Zeus Group A), light (weapon system delivery missiles), and heavy (LV-3/Agena) Atlas launch vehicle configurations to determine the demands placed upon the rate gyros in flight. Fig. 15 presents the magnitude of the rate gyro excursions obtained from telemetry records of 65 flight articles (4 Nike-Zeus, 51 weapon system delivery, and 10 Agena). These data do not include the roll program rates.

b. Transfer Function

As seen in Eq. (35), the response of a rate gyro (Fig. 16) can be adequately represented by the characteristic second-order transfer function.

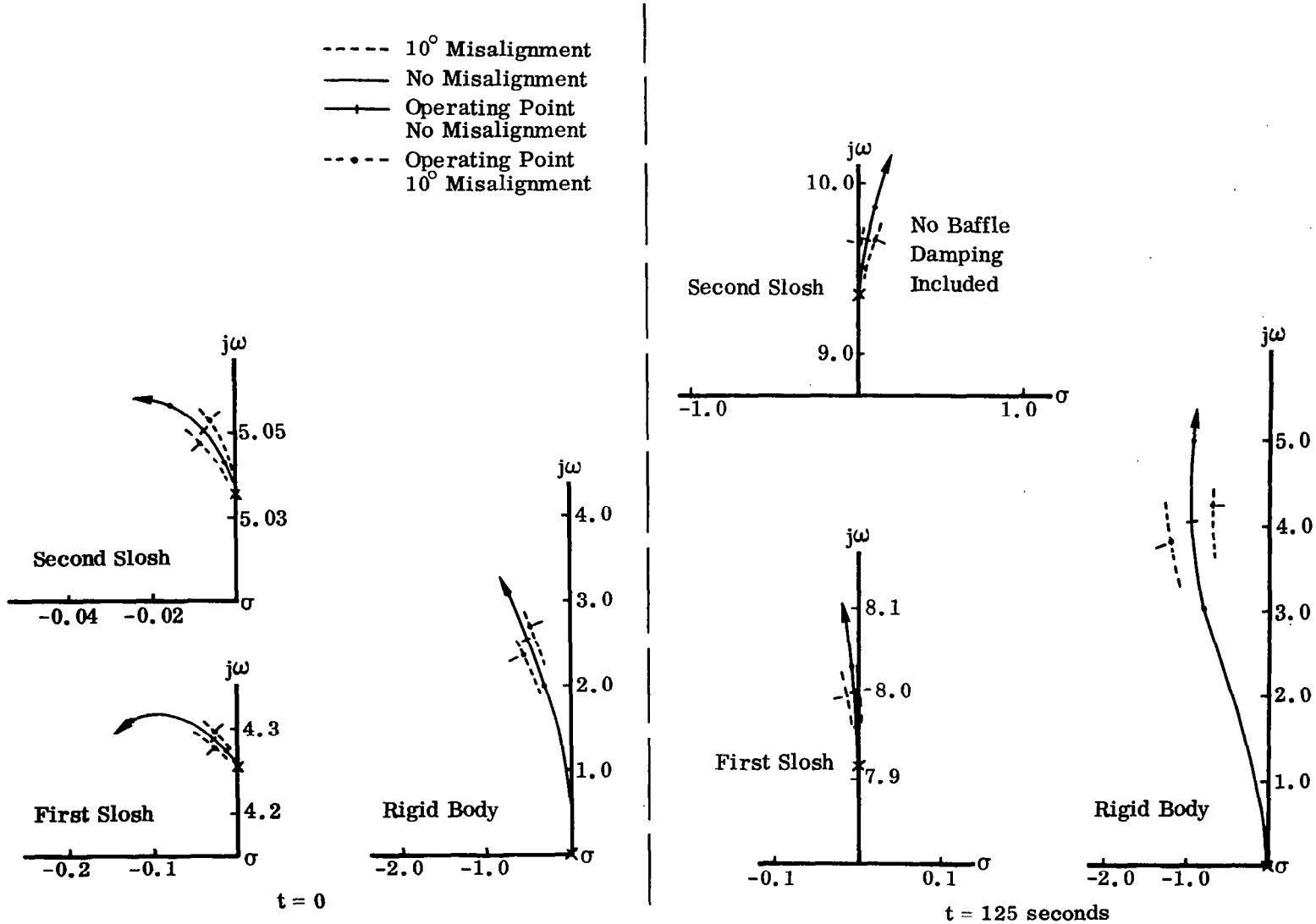

Figure 14. Typical Root Loci Showing Effect of Pitch and Yaw Coupling Due to Noncongruity (Rate Gyro)

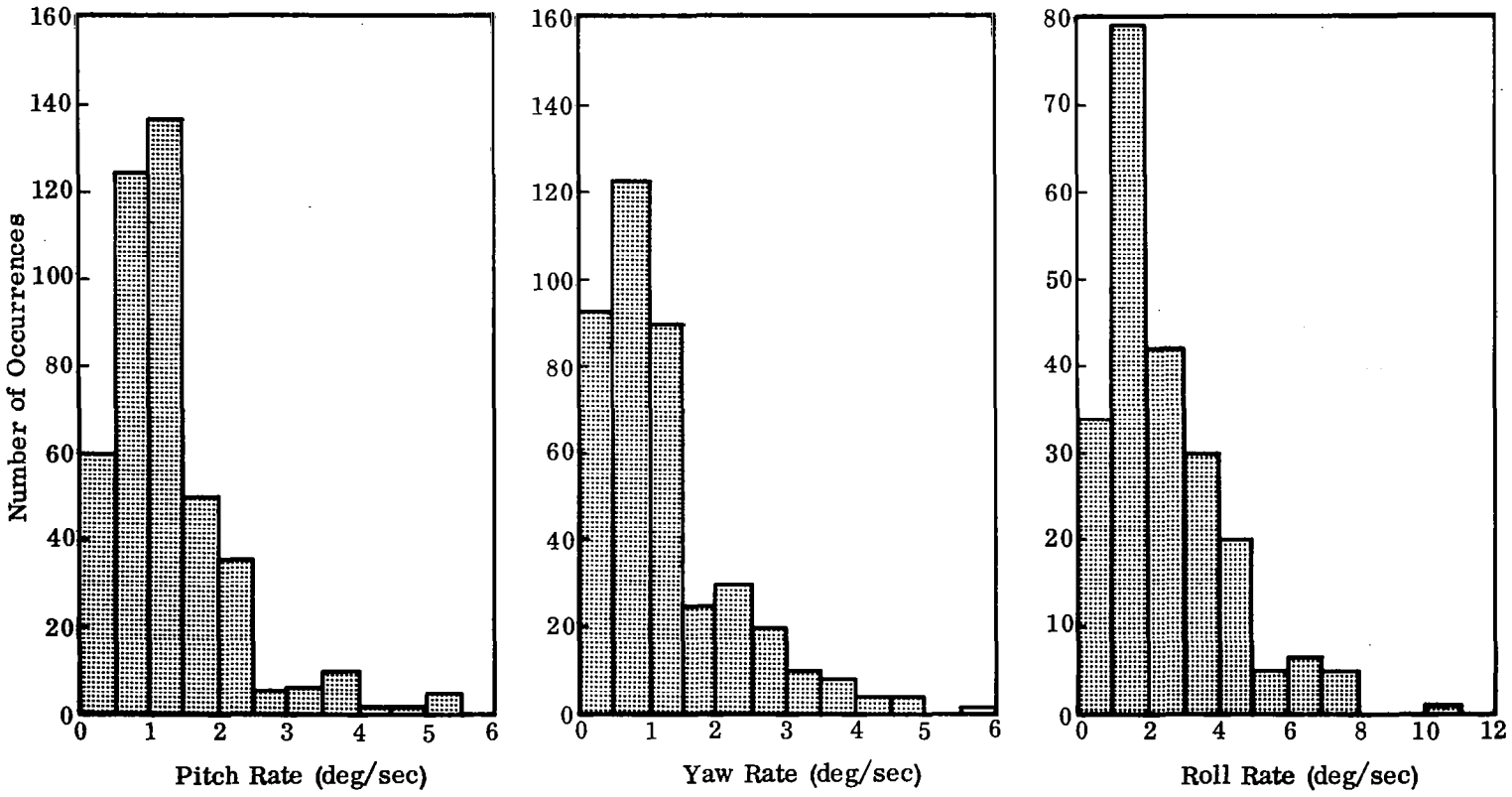

Figure 15. Maximum Excursion Histograms, Rate Gyro

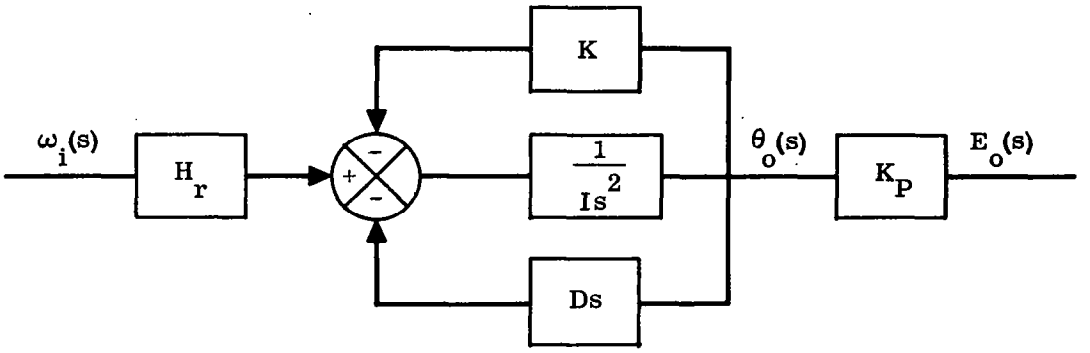

Figure 16. Rate Gyro Block Diagram

$$\frac{E_o}{\omega_i}(s) = \frac{K_R}{\frac{s^2}{\omega_R^2} + \frac{2\zeta_R}{\omega_R} s + 1} \tag{43}$$

where

$$E_o = K_P \theta_o$$

$$K_R = K_P H_r / K$$

The dynamic response requirements and required damping characteristics largely determine the rate gyro undamped natural frequency. If the desired response is flat or has a minimal phase shift to some frequency, then ω_R should be approximately 1.4 times that frequency. If dynamic inertial coupling is present, ω_R should be even higher, so that when the effects of dynamic natural frequency depression are included, the apparent ω_R will still be high enough.

The frequency to which a flat gyro response is desired should be that of the highest frequency/phase-stabilized bending mode, ω_B.

With the application of a factor of two to allow for dynamic coupling, etc., a plausible natural frequency appears to be

$$\omega_R > 2\,(1.4)\,\omega_B$$

In general, the advantages of high-natural-frequency gyros are:

a. Less amplitude and phase uncertainty over a broader frequency range.

b. Better environmental resistance, primarily in gyros with integral gimbal suspension and restraint. (Increasing ω_R increases the gyro spring constant, which, in turn, increases the transverse stiffness of the gimbal support.)

c. Low crosstalk.

d. Low torsion spring stress.

The disadvantages are:

a. Small pickoff output; θ is inversely proportional to ω_R^2.

b. The gyro may respond to unwanted high-frequency rate components.

The latter factor should not constitute a major difficulty, since large high-frequency attenuation is usually provided by other control system components.

The upper limit of the damping ratio can be determined by observing the phase uncertainty relative to some selected minimum, ζ_R. For example, assume $\zeta_{R_{min}} = 0.40$ at $\omega_B = 40$ rad/sec for a given ω_R. Now say that a value of $\zeta_R = 0.80$ yields a phase band on the order of 15° at the same ω_B. This 15° phase uncertainty can be handled by phase stabilization in compensating for an elastic mode. Then, the range $0.40 \leq \zeta_R \leq 0.80$ would provide acceptable damping ratios.

For rate gyros used in a roll channel, the requirements are more flexible. The parasitic modes in the roll plane (torsional modes) occur at relatively high frequencies (12 to 15 cps and higher); consequently, the rigid-body control mode (frequency range of 0 to 2.5 cps) is the only mode of concern. In the absence of lower parasitic modes, precise electronic stabilization networks are not required. The primary requirement is to roll off the system response at a frequency less than the fundamental torsional mode. This flexibility, inherent in most roll channels, precludes the need for specific requirements (ζ_R and ω_R) for the roll rate gyro dynamic characteristics. Gyro selection may be made simply by examining the dynamics of the gyros and making recommendations based on the roll channel implementation required.

It is also possible to obtain rate information from a rate integrating gyro. This is accomplished by placing a nulling amplifier around the gyro such that the output becomes proportional to angular rate. As an example, consider the rate integrating gyro of Fig. 10, with a feedback signal, K_F, as shown in Fig. 17.

Let

$$E_i = -K_F E_o$$

Then Eq. (41) becomes

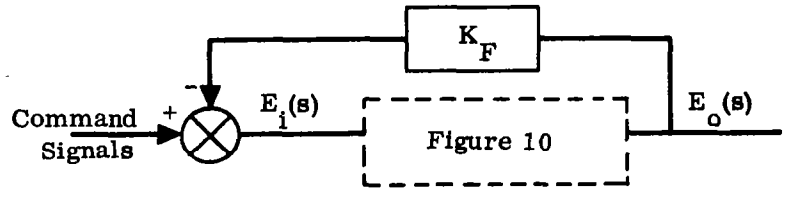

Figure 17. Rate Information From a Rate-Integrating Gyro

$$E_o = \frac{1}{s} \frac{K_P/D}{(I/D)s + 1} \times \left[H_r \omega_i - K_F K_T G_T(s) E_o \right] \qquad (44)$$

This reduces to:

$$\frac{E_o}{\omega_i} = \frac{K_P H_r}{Is^2 + Ds + K_F K_P K_T G_T(s)} \tag{45}$$

which is the gyro output/input rate transfer function.

It can be seen that the electric restoring force ($K_F K_P K_T G_T$) is equivalent to the spring K in Eq. (43) for a spring-restored rate gyro. The damping of this second-order system depends upon the feedback gain (hence frequency) chosen.

As in displacement gyros, there is some level of input (threshold) to a rate gyro below which the output will not track the input. In addition, some output (null offset) can be expected with zero input rate, since the gyro output device cannot be precisely aligned with the spring restraint. Thresholds are usually accepted at relatively low values ($< 0.02°$/sec), below those of control-actuating systems. Their effect on stability is mostly negligible. The effect of a null offset is identical to that of a constant displacement error, where the signal is added to that of the attitude reference. A guidance command of some sort may be required to cancel out this error.

3.1.2 Accelerometers

Although not widely used as primary sensing elements for the stability and control of launch vehicles, accelerometers are included here because they form an integral part of platforms. At least one vehicle[2] employs a form of accelerometer to provide angular rate information.

Most accelerometers are based on a common principle of operation: the measurement of the motion of a restrained mass when it is subjected to acceleration. Variation of parameters allows some instruments to be used to measure acceleration, velocity, and displacement, depending on the implementation of the basic principle and on the portion of the frequency range employed.

3.1.2.1 Seismic Accelerometers

A typical elastic-constraint type of accelerometer is a proof mass suspended by a spring that obeys Hooke's Law. The deflection of the spring is proportional to the applied acceleration. This type of accelerometer is representative of the basic principle of operation and is shown functionally in Fig. 18 as a damped spring-mass system.

Summing up the forces acting on the mass:

$$M(\ddot{R} - \ddot{X}) = KX + D\dot{X} - Mg \qquad (46)$$

Rearranging, we have, in Laplace notation,

$$\frac{X}{A_i}(s) = \frac{M}{Ms^2 + Ds + K} \qquad (47)$$

where A_i represents the total input acceleration ($\ddot{R} + g$), to the instrument. Therefore, in standard form, we have

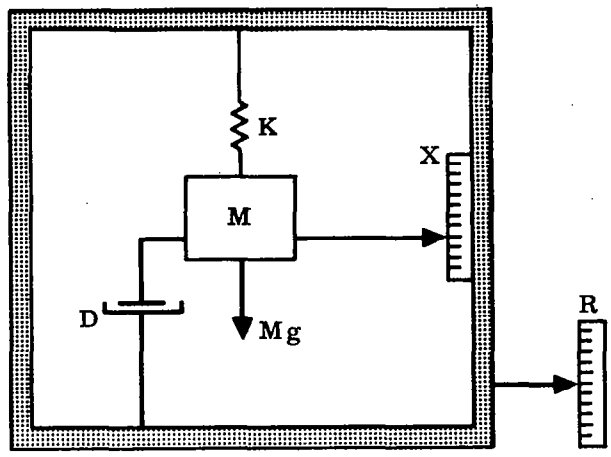

Figure 18. Accelerometer Schematic

$$\frac{X}{A_i} = \frac{1}{s^2 + 2\zeta\omega s + \omega^2}$$

where

$$\omega = \sqrt{K/M} = \text{natural frequency}$$

and

$$\zeta = \frac{D}{2}\sqrt{K/M} = \text{damping ratio}$$

Including the sensitivity, K_s, as the third parameter required to specify the response, we have the overall accelerometer transfer function:

$$\frac{X}{A_i} = \frac{K_s}{s^2 + 2\zeta\omega s + \omega^2} \qquad (48)$$

Given a high spring constant, K, the output, X, is proportional to A_i, and the instrument is a true accelerometer measuring total acceleration. If the damping provided is sufficiently high that the Ds term predominates, the output is proportional to $\int A_i\,dt$, and we have an integrating accelerometer (velocity meter). A high Ms^2 term yields an output proportional to $\int\int A_i\,dt$ for a double integrating accelerometer (distance meter).

The natural frequency, $\sqrt{K/M}$, applies to systems where the damping has no effect on either the spring constant or the suspended mass. In a fluid-damped system, a fluid mass must be moved by the proof mass to obtain the required damping. The frequency of such a system[1] can be approximated by

$$\omega = \sqrt{\frac{K}{M + m\left(A_1/A_2\right)^2}} \tag{49}$$

where

A_1 = area of proof mass

A_2 = area of fluid in space around the proof mass

m = mass of fluid in space around the proof mass

The accuracy of these spring-mass instruments depends largely on the accuracy of the spring. Nonlinearities, hysteresis, and other properties of the spring result in output errors. Thus these instruments are generally less accurate and have a smaller range than the force-balance or servo types.

The accelerometer can also be adapted to record linear and/or angular acceleration in all combinations. Consider the instrument shown schematically in Fig. 19.

The equation of motion can be determined by equating the inertial moments, I, and the base moments, B, due to restraints K, the gimbal spring, and D, the damper.

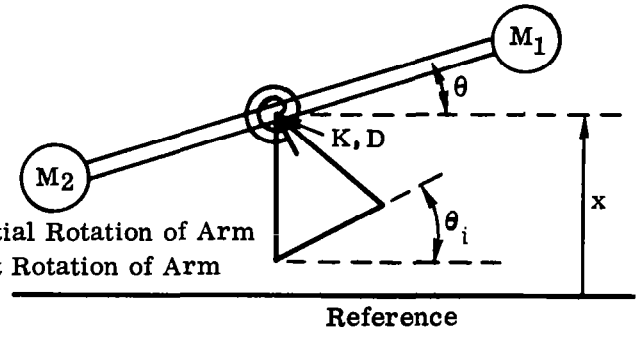

Figure 19. Spring-Rebalance Accelerometer

$$\Sigma M_{\theta_{(I)}} = M_2 \ell_2 \ddot{x} - M_2 \ell_2^2 \ddot{\theta} - M_1 \ell_1^2 \ddot{\theta} - M_1 \ell_1 \ddot{x} \tag{50}$$

$$\Sigma M_{\theta_{(B)}} = D\left(\dot{\theta} - \dot{\theta}_i\right) + K\left(\theta - \theta_i\right) \tag{51}$$

Equating and solving these two equations,

$$\theta = \frac{\left(Ds + K\right)\theta_i + \left(M_2 \ell_2 - M_1 \ell_1\right)s^2 x}{\left(M_2 \ell_2^{\,2} + M_1 \ell_1^{\,2}\right)s^2 + Ds + K} \tag{52}$$

Now let the output voltage

$$E_o = k\left(\theta_i - \theta\right) \tag{53}$$

and place the accelerometer a distance L from the center of gravity of a body such that

$$\ddot{x}_a = \ddot{x} + L\,\ddot{\theta}_i \tag{54}$$

where x_a = total displacement at the accelerometer location.

Placing (53) and (54) in (52) results in the transfer function:

$$\frac{E_o}{k} = \frac{\left[\left(M_1 \ell_1^{\,2} + M_2 \ell_2^{\,2}\right) + L\left(M_2 \ell_2 - M_1 \ell_1\right)\right] s^2\theta_i + \left(M_1 \ell_1 - M_2 \ell_2\right)s^2 x_a}{\left(M_1 \ell_1^{\,2} + M_2 \ell_2^{\,2}\right)s^2 + Ds + K} \tag{55}$$

Thus the accelerometer can be made to sense either $\ddot{\theta}$ or $\ddot{x}$ or any combination of the two by adjusting the masses and distances.

3.1.2.2 Force-Balance Accelerometers

These accelerometers (Figs. 20 and 21) consist essentially of a mass that moves along an acceleration-sensitive axis and a device to measure the motion of the mass. The output resulting from the motion is fed to a high-gain amplifier whose output current flows through a force-balance coil that forces the displaced mass back to its original null position. In effect, the instrument is a high-gain, null-seeking servo in which the force-balance coil current is proportional to the acceleration applied.

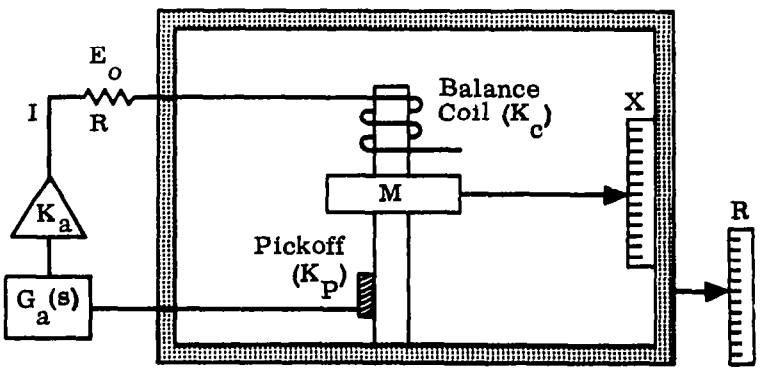

Figure 20. Schematic of Force-Balance Accelerometer

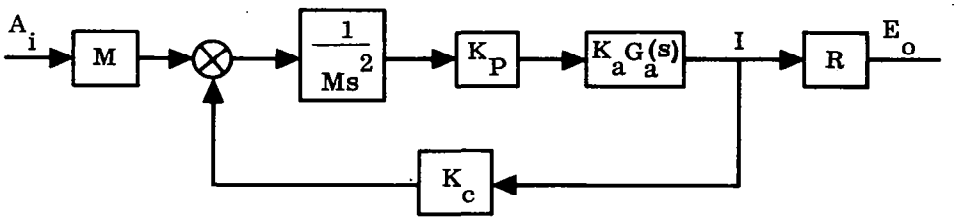

Figure 21. Block Diagram for Figure 20

The closed-loop system is characterized by the following transfer function.

$$\frac{E_o}{A_i} = \frac{R K_P K_a G_a(s)}{s^2 + \frac{K_P K_c K_a}{M} G_a(s)} \tag{56}$$

where G_a (s) is the transfer function of the stabilization (or shaping) network, typically a lag-lead network such as

$$\frac{(\tau_1 s + 1)(\tau_2 s + 1)}{(\tau_3 s + 1)(\tau_4 s + 1)}$$

Since this type of accelerometer always operates about null, a very high degree of linearity can be made available. Accuracies of 0.0001g are within the capability of a nonpendulous type, while still lower thresholds are available from pendulum accelerometers.

Such an analog force-balance type of accelerometer can be modified so that it is pulse-torqued, providing an output that is essentially digital. In operation, current pulses flow through the force-balance coil at a repetition rate proportional to acceleration. If these pulses are counted for a fixed period of time (say 0.1 second), the accumulated count is proportional to the average acceleration over that time interval. If each pulse has the same energy, the pulse rate is proportional to acceleration. Since each pulse effectively represents a fixed increment of velocity, the instrument can furnish velocity data simply by counting pulses. Potentially, such accelerometers are even more accurate than their analog counterparts.

3.1.2.3 Pendulous Gyroscope Accelerometers

A pendulous integrating gyro accelerometer is a single-axis gyroscope with an intentionally large mass unbalance along its spin axis. An acceleration along the input axis causes motion about the precession axis. Mounted in a gimbal, on its own single-axis platform, the gyro is part of a null-seeking servo loop in which motion about the precession axis is detected and fed to a torquer to cause relative motion

between the gimbal and the platform. With a mass unbalance, m, an acceleration, A_x, along the input axis creates an output-axis torque, mA_x. To maintain the pickoff angle, θ, at null, the gyro is made to rotate about its input axis with angular velocity

$$\dot{\phi}_x = \left(m/H_r\right) A_x \tag{57}$$

Therefore

$$\phi_x = \frac{m}{H_r} \int A_x \, dt \tag{58}$$

which makes the instrument a velocity meter.

A unique advantage of this type of accelerometer is its freedom from any Hookean type of restraint. Linear, unsaturable torque attributable to the pendulous element is balanced by a similarly unsaturable linear torque developed by the gyro's precession.

3.1.3 Platforms

The principal function of a stable platform is to establish and maintain a reference coordinate system with respect to space. To isolate it from the angular motions of the vehicle, the platform is mounted in a gimbal system that permits angular disturbances. Gyroscopes provide the orthogonal reference to which the platform is oriented. This orientation is maintained through a system of servos, or a platform controller. Therefore, a platform can be described as a cluster of gyros mounted within gimbals that are controlled by the outputs of the gyros through servo loops. A great variety of platform types can be produced by various arrangements of gimbals and gyros. A detailed study of such a complex instrument is obviously beyond the scope of this monograph. The treatment here is restricted to a cursory look at platform representation in stability and control loops.

Fig. 3 illustrates a typical single-axis platform using an SDOF gyro. The gyro input and output transfer functions, Eqs. (32) to (34), were based on the same platform-mounted gyro. Referring again to the figure and equations, stabilization of the platform is accomplished by using the pickoff angle between the gyro gimbal and the platform to drive the platform servocontroller. Fig. 22 shows schematically a simplified stabilization or alignment loop for such a platform. The symbols used are defined in the same manner as those employed in Eqs. (32) and (33). Like all servo loops, the alignment loop is subject to the same criteria of stability and response over a range of operating frequencies. The diagram is basic and does not include the compensating functions required to ensure adequate damping and gain and phase margins. Command inputs refer to those employed to control the platform motion. Examples of these are: constant "earth-rate signal" to rotate the platform at the angular velocity of the earth, thereby keeping the platform fixed relative to earth; and a variable signal

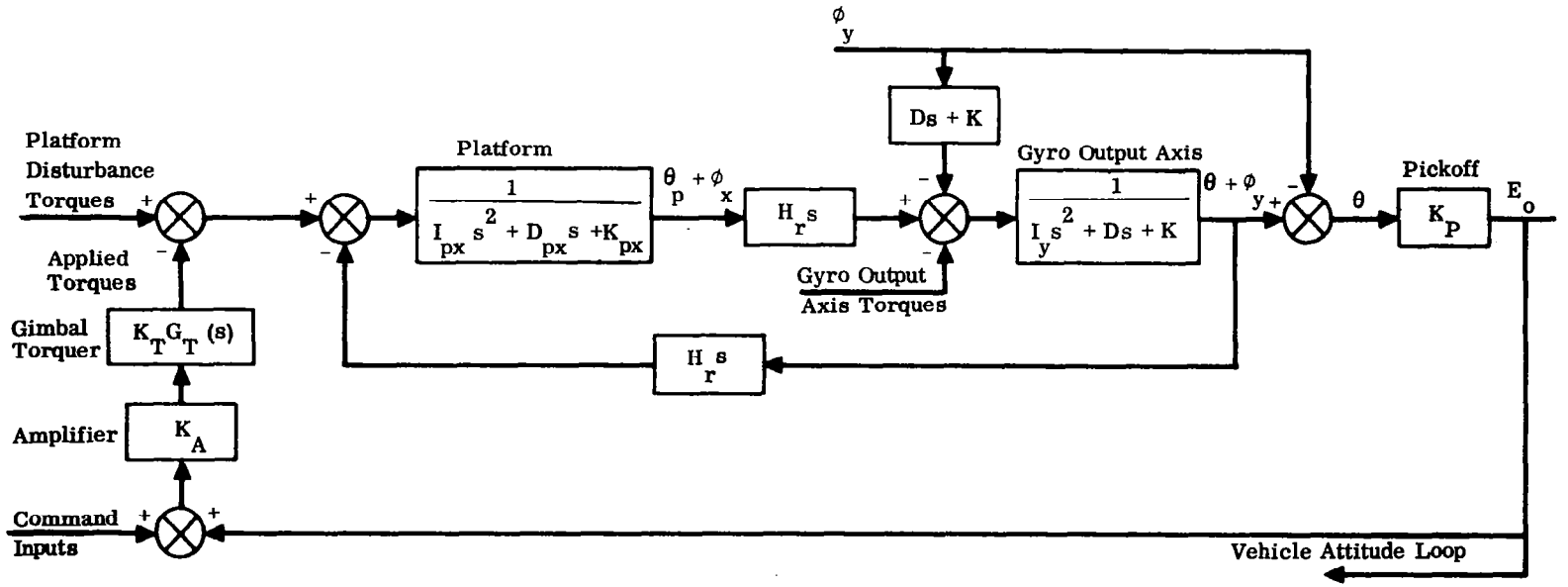

Figure 22. Simplified Stabilization Loop for a Single-Axis Platform

applied as a function of acceleration to rotate the platform at a rate proportional to acceleration.

The single-axis platform was used for simplicity as an illustration of the functioning of the gyro-stabilized platform. In general, the three-axis reference system is provided by two TDOF or three SDOF gyros mounted on three- or four-gimbal platforms. The analysis of these systems is complicated by many problems, including that of interaxis coupling where disturbances from one loop are coupled into another loop.

From a practical standpoint, platform responses tend to be nonlinear; the effects of friction are particularly pronounced at low signal levels, where the platforms are usually operating. However, platforms are generally considered as "stiff" systems and, for low frequencies, can be linearized without very much error. For example, the transfer function,

$$\frac{\theta_o}{\theta_i} = \frac{\left(\tau_2 s + 1\right)}{\left(\tau_1 s + 1\right)\left(\frac{s^2}{\omega_n^2} + \frac{2\zeta}{\omega_n} s + 1\right)} \tag{59}$$

proved to be a good linear approximation to data provided by a manufacturer. (See Fig. 23.)

For the stability and control of elastic vehicles, a simple transfer function like the one above may not suffice. More details may have to be introduced in the analysis. Normally, the bending mode is not included in the position loop, but for configurations where the slope of the first bending mode at the platform location is high with respect to the slope at the rate sensor location, an appreciable component of the mode can be expected to register. This should be kept in mind for all vehicles where the position and rate sensors are at different locations, particularly when the position sensors are located in one of the upper stages of a multistage vehicle. Fig. 24 is a typical single-plane block diagram for the analysis of such a configuration with the vehicle and platform angles defined in Fig. 25.

3.1.4 Angle-of-Attack Sensors

The list of possible techniques for measuring angle of attack (α) is quite long, and no attempt will be made here to provide a complete set of descriptions. Ref. 5 gives descriptions and primary evaluations of many of the ideas advanced for α measurements. This discussion will confine itself to only a few typical methods based on "direct" sensing.

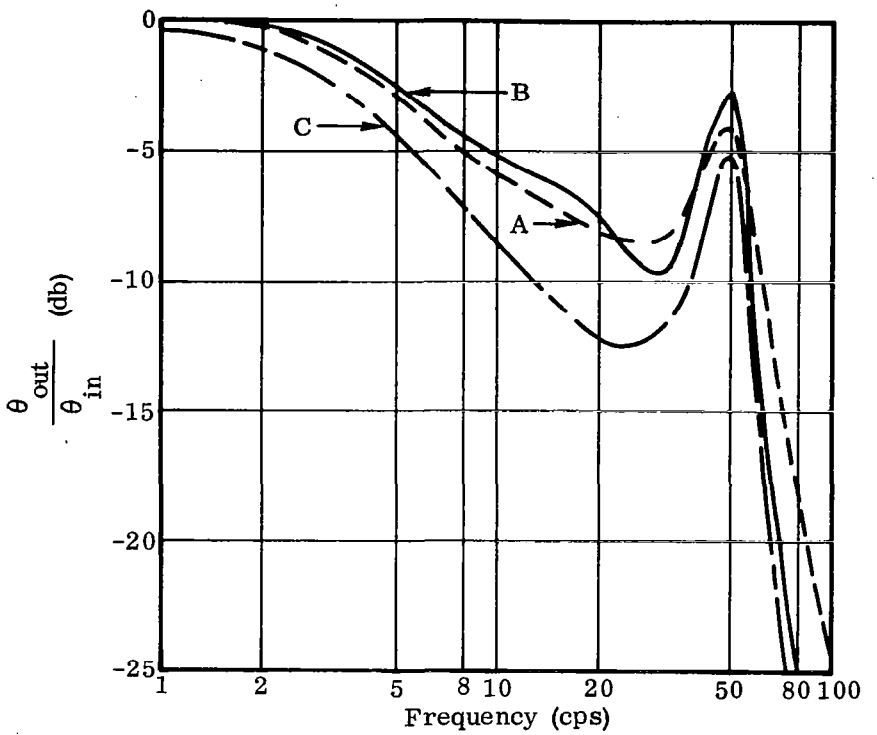

Curve A - Square Wave Response (Manufacturer's Data)
Curve B - Approximate Square Wave Response } Computer Model
Curve C - Approximate Sine Wave Response }

Figure 23. Platform Frequency Response (Bode Plot)

A basic principle used in stationary sensors is illustrated in Fig. 26. Since α is normally obtained from the pressures of two or more appropriately positioned orifices, one may write

$$\alpha = K \frac{P_U - P_L}{P_T - P_S} f(M)\, f(\beta) \tag{60}$$

where

K = an appropriate constant

M = the free-stream Mach number

β = the sideslip

$P_T - P_S$ = the measure of dynamic pressure, q

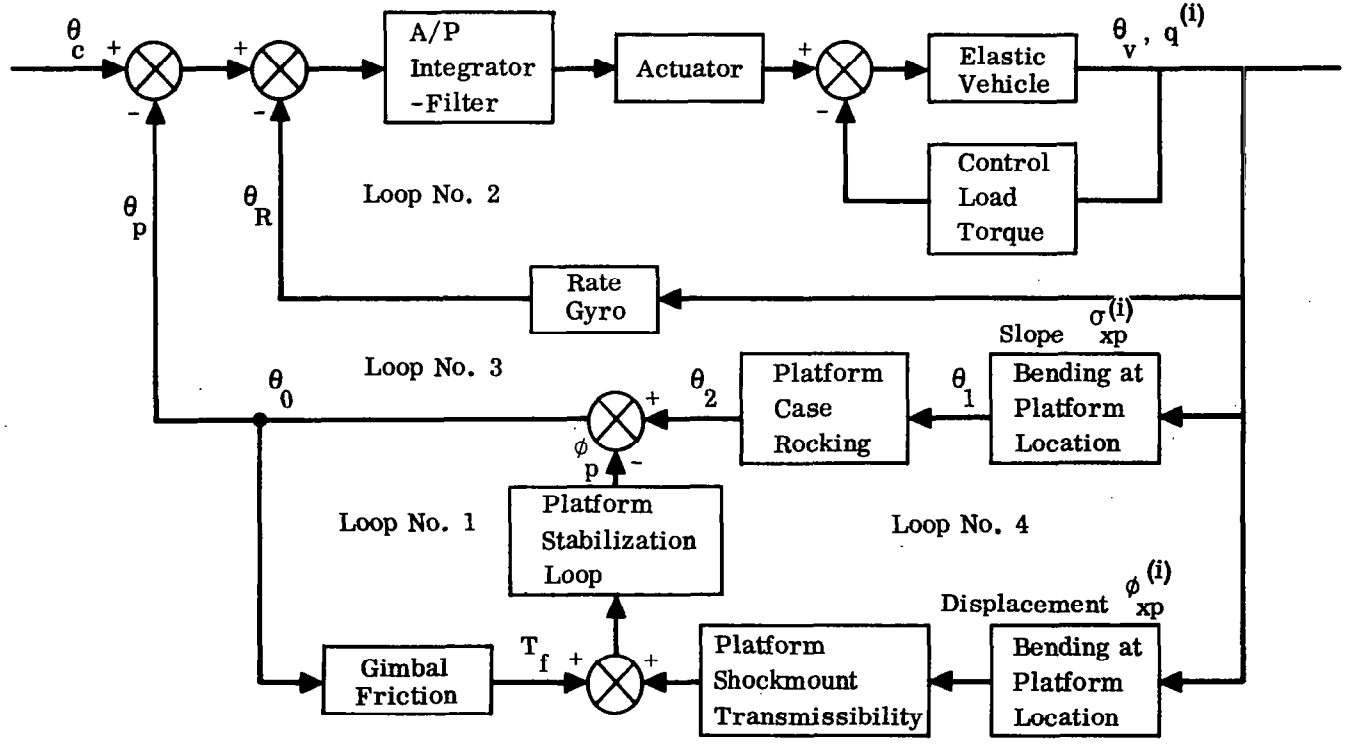

Loop No. 1	Gimbal Friction
Loop No. 2	Rate Gyro Feedback
Loop No. 3	Platform Attitude Reference
Loop No. 4	Platform Mass Unbalance Effect on Attitude Reference

θ_c - Command Attitude Angle

θ_p - Position Feedback Signal

θ_R - Rate Gyro Feedback Signal

Figure 24. Single-Plane Block Diagram for Vehicle Autopilot Control Loop

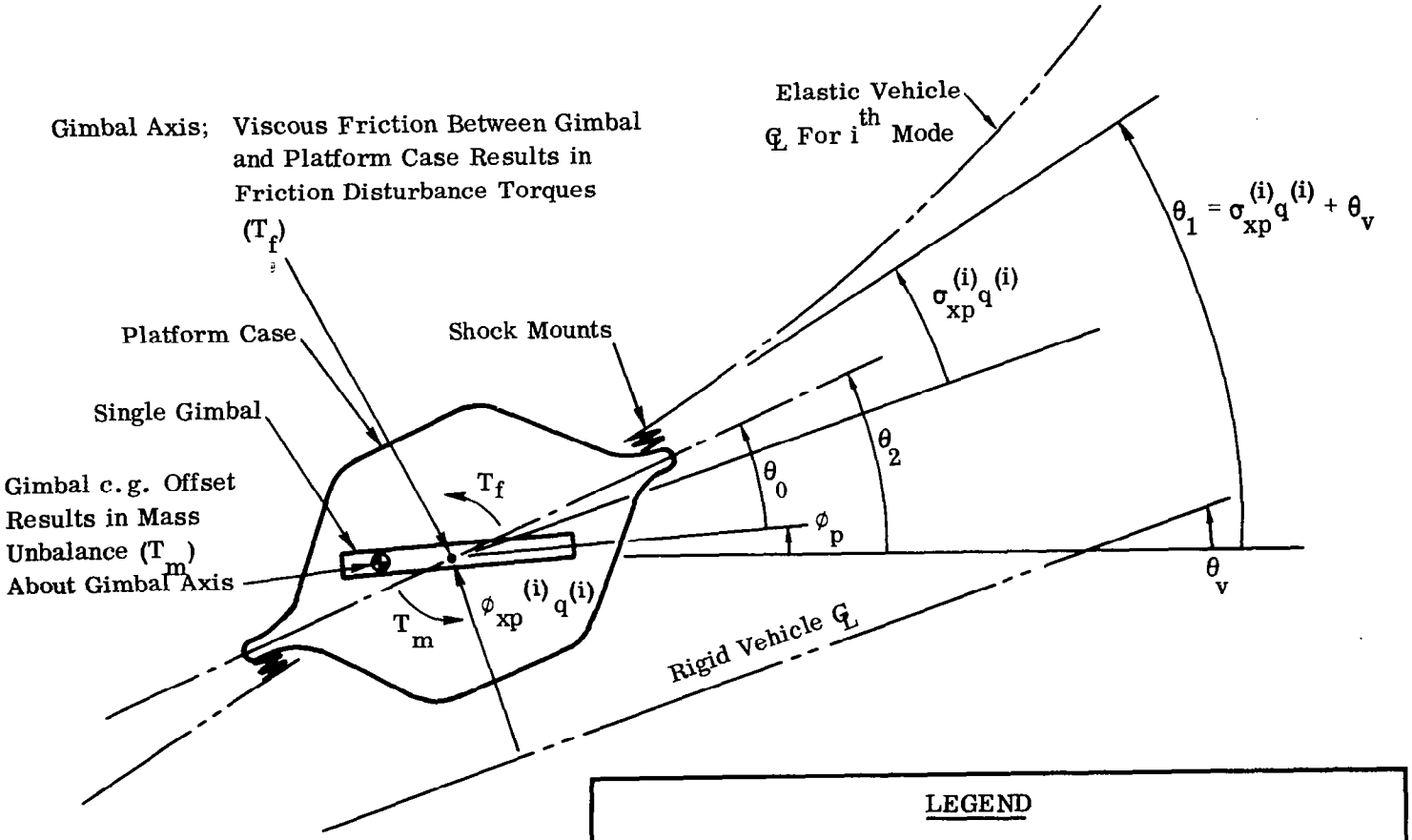

LEGEND

- θ_v - Vehicle Angular Displacement Relative to Reference Axis.
- θ_1 - Vehicle Attitude at Platform Location (Rigid + Elastic).
- θ_2 - Platform Case Attitude.
- ϕ_p - Inertial Platform Rotation Resulting from Disturbance Torques, T_m and T_f.
- θ_0 - Vehicle Attitude as Read by Gimbal Resolvers.

Figure 25. Definition of Vehicle and Platform Angles

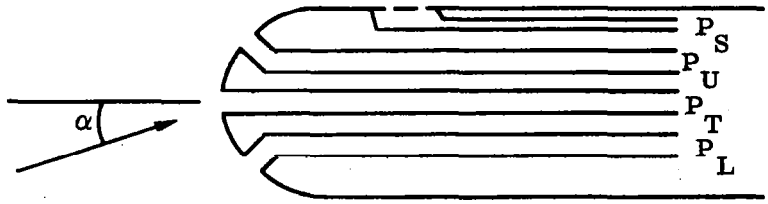

Figure 26. Stationary Angle-of-Attack Sensor

With this type of probe, first-order dynamic requirements apply only to the measurement of $(P_U - P_L)/q$. Dynamic pressure and Mach number vary slowly compared with the short-period variation of α. The function of β cannot be neglected, since it does have short-period characteristics. One method of compensating is to mechanize the function as a change in the gain of the α-sensor. The permissible lag resulting from this β correction will depend on the amount of dynamic crosstalk that can be tolerated.

The transfer function that operates directly on α depends on the pressure-ratio-sensing mechanism and the pneumatic characteristics of the probe, lines, and transducer volume.

The easiest way to get good dynamic response for pressure-ratio measurements is to drive transducers directly from bellows volume. The pneumatic line lag can be approximated by a first-order time constant

$$\frac{1}{\tau_\ell s + 1}$$

where

$$\tau_\ell = \frac{128\,\mu\ell}{P\pi D^4}\left(V + \frac{V_t}{2}\right)$$

μ = the air viscosity

P = the average pressure in the system

$V_t = \pi \ell D$ = the volume of the sensing line

V = the transducer volume

In addition to this lag, there is a transportation time delay that becomes significant only with long pneumatic lines between the sensor and the transducer.

Including the time constant of the bellows transducer (τ_b), the transfer function for the sensor is given by

$$\frac{\alpha_m}{\alpha} = \frac{K e^{-as}}{(\tau_\ell s + 1)(\tau_b s + 1)} \tag{61}$$

where

K = an arbitrary constant

a = the line transport time delay

τ_ℓ = the pneumatic line lag

τ_b = the time constant of the bellows-transducer

α_m = the measured angle of attack

With the small volumes associated with these instruments, extreme accuracies cannot be obtained, because the measured pressure ratio must be high enough to overcome friction in the system. Both response and accuracy deteriorate at low values of q.

Servo-driven pressure-ratio sensors offer potentially higher accuracy. Replacing the bellows transducer above with a q-sensitive servo loop yields an equation of the form

$$\frac{\alpha_m}{\alpha} = \frac{K_1 e^{-as}}{(\tau_\ell s + 1)\left[\frac{\tau_m}{K_s} s^2 + \left(\frac{1}{K_s} + K_T\right)s + 1\right]} \tag{62}$$

where

K_1 = an arbitrary constant ($\neq K$)

τ_m = the servomotor time constant

K_s = the servo gain, a function of q

K_T = the servo rate feedback gain

The moveable sensor is usually designed to point into the relative wind, with the angle of attack being derived from its position relative to the airframe. This class of sensors can be subdivided into simple vane types and powered null-seeking devices. The two are similar in that α is read from the position of the sensor.

The aerodynamic-vane type presents a simple and reliable solution to α measurement. Accuracies of 1/4° or less are attainable at supersonic speeds. Subsonic operation brings upwash errors, which can be as high as 1° at a 5° angle of attack. The latter is a position error and can be compensated for as a function of Mach number.

A typical example of this type of sensor is a straightforward NASA design[10] shown schematically in Fig. 27. Its transfer function is given by

$$\frac{\theta}{\alpha}(s) = \frac{\dfrac{C_{L_{\dot{\alpha}_v}}}{C_{L_{\alpha_v}}} s + 1}{\dfrac{I}{q A x C_{L_{\alpha_v}}} s^2 + \left(\dfrac{C_{L_{\dot{\alpha}_v}}}{C_{L_{\alpha_v}}} + \dfrac{F\,(\text{Ampl.})}{q A x C_{L_{\alpha_v}}} \right) s + 1} \tag{63}$$

where

$$C_{L_{\dot{\alpha}_v}} = \frac{\partial C_L}{\partial \dot{\alpha}_v}$$

$$C_{L_{\alpha_v}} = \frac{\partial C_L}{\partial \alpha_v}$$

I = moment of inertia about H_L

x = distance from the center of pressure to H_L

$F\,(\text{Ampl.})$ = effective damping from friction

θ = the vane position relative to the vehicle reference

α_v = the angle of attack of the vane

The light weight of this vane contributes to its good characteristics in terms of damping and frequency.

Potentially greater accuracies may be attainable with the null-seeking, servo-driven, moveable sensor. The device has a pair of orifices located symmetrically about a reference axis and is driven by a servo so that pressures on the two orifices are equal. Since the servo is usually located near the probe, pneumatic lags are negligible. The range of differential pressure to be measured need not be large; hence good dynamic response can be expected. The characteristics of this type of sensor should be dominated by those of the servo that drives the null-seeking head. Typically,

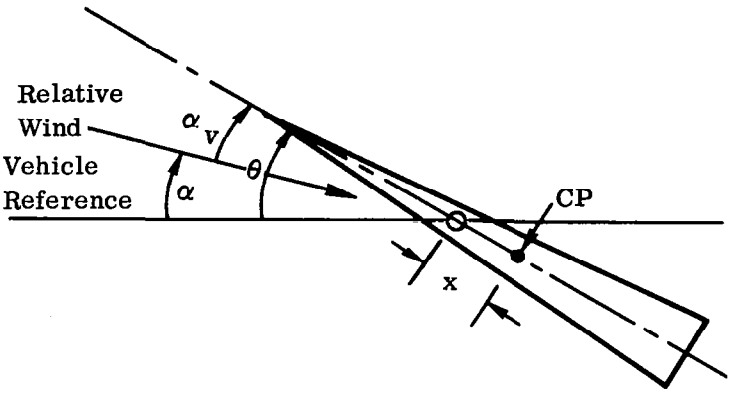

Figure 27. Aerodynamic, Vane-Type α-Sensor

$$\frac{\theta}{\alpha}(s) = \frac{K}{\frac{\tau_m}{K_s} s^2 + \left(\frac{1}{K_s} + K_T\right) s + 1} \tag{64}$$

K_s is a function of q. Unless some gain-scheduling is provided, the servo should be designed with adequate response set by the lowest dynamic pressure to be encountered, and stability should be determined by the highest. The transfer function varies from heavily damped, essentially first-order response at low q values to highly damped, second-order response at high q's.

It should be noted that α is the total angle measured at the sensor location.

$$\alpha_{vehicle} = \alpha_{rigid} - \sum_i \sigma^{(i)} \ell_m q^{(i)} \tag{65}$$

where

$\sigma^{(i)}$ = negative slope of the i^{th} bending mode in the plane of the sensor

ℓ_m = distance from the vehicle c.g. to the sensor location

$q^{(i)}$ = generalized coordinate of the i^{th} bending mode

3.2 ACTUATING ELEMENTS

The function of an actuator in a servo system is to provide the motive power to the control element (vehicle controls). The selection of an actuating device, therefore, is determined primarily by the power requirements of the control load. Other factors to be considered include the dynamic characteristics, the power sources available, and the physical and economic limitations of the equipment as well as its reliability.

Actuators generally available for application to launch vehicle systems fall into three broad categories: electrohydraulic, electromechanical, and pneumatic. The last two have found only limited usage, mainly in small missiles. The weight, space, and power required by electric motors to move large control loads make them rather unattractive except under highly restrictive conditions. The problems attendant to pneumatic systems center about their relatively lower frequency resonance and their lack of fine positioning accuracy.

The electrohydraulic servo represents a good compromise of the characteristics generally required for control actuation in launch vehicles and therefore has gained the widest acceptance in the industry.

3.2.1 Electric Motors

Because of the abundance of literature available on electric motors, the discussion here will be restricted to a few general remarks regarding their characteristics.

A-c motors are usually employed for the smallest power requirements, up to approximately 100 watts. They can be disregarded when considering the types of control elements involved in launch vehicles, although they are capable of moving sizable loads over small distances. The transfer function for these motors has the general form

$$\frac{\theta}{E_i} = \frac{K}{s(\tau s + 1)} \tag{66}$$

where

E_i = the input voltage

θ = the output shaft position

K = the motor constant

τ = the motor time constant

Addition of feedback elements yields a second-order position servo.

D-c motors are more generally used in larger power applications, since they can generate higher torques more efficiently. In addition, they offer larger power/volume ratios. For a given set of torque and velocity requirements, the armature-controlled (shunt) motor will usually give the fastest dynamic response. A field-controlled unit provides good economy of control power but lacks inherent damping and is useful only when slow response can be tolerated. It is also inefficient in overall use of electrical power, since high armature currents must be maintained for proper control, regardless of output. The servo using a series motor would probably best meet the needs of the majority of direct-coupled electrical control actuation requirements. It provides the highest stall and low-speed torque for a given motor weight.

The transfer functions for the three types are essentially of the same form, a third order that can be simplified by neglecting armature and field inductance. For the series motor, the linearizing process used to arrive at the third-order transfer function involves extreme assumptions of proportionality; therefore the results are good only for small disturbances about some specific operating point.

3.2.2 Pneumatic Actuators

The following definitions and symbols are used in this section.

A_h	Effective orifice area	$in.^2$
Ai_{10} (Ai_{20})	Average effective inlet area from extend (retract) side of the cylinder	$in.^2$
Ae_{10} (A_e20)	Average effective exhaust area from extend (retract) side of the cylinder	$in.^2$
A_1 (A_2)	Piston area on extend (retract) side	$in.^2$
C	The negative of the partial of the nonlinear flow coefficient, N, with respect to pressure ratio	N.D.
C_d	Discharge coefficient of orifice	N.D.
$f(\dot{\delta})$	A generalized friction representation	in.-lb/rad/sec
g	Acceleration due to gravity	368 in./sec/sec
i	Valve input	milliamp
I_R	Load moment of inertia as seen by the actuator	$lb\text{-}in.\text{-}sec^2$
K_i	Valve input gain	$in.^2/ma$
K_M	Mounting structure spring constant	lb/in.

K_R	Load spring constant	in.-lb/radian
m	Mass of gas	lb-sec^2/in.
n	Polytropic index	N.D.
P	Absolute pressure	psi
P_1 (P_2)	Absolute pressure in extend (retract) side of actuator	psi
P_{10} (P_{20})	Average pressure in extend (retract) side of actuator	psi
P_d	Downstream pressure	psi
P_u	Upstream pressure	psi
P_s	Supply-source pressure	psi
P_L	Load pressure (= $P_1 - P_2$)	psi
R	Length of lever arm	in.
R_g	Ideal gas constant ---- for air ---- for most solid propellants	640 in./°R 900 in./°R
r	Ratio of downstream to upstream pressure to just give sonic flow in an orifice (0.53 for most gases)	N.D.
T	Absolute temperature	°R
t	Time	sec
V	Volume	in.^{3}
V_{10} (V_{20})	Average volume in extend (retract) side of cylinder	in.^{3}
W	Weight rate of flow of gas	lb/sec
W_{1c} (W_{2c})	Weight rate of flow of gas into the extend (retract) side of the actuator	lb/sec
W_{1v} (W_{2v})	Weight rate of flow of gas from the extend (retract) side of the valve	lb/sec
x	Position displacement	in.
W_{01} (W_{02})	Weight rate of flow of gas from supply port through exhaust port during steady-state null position of valve and actuator	N.D.
γ	Ratio of specific heats of power fluid	N.D.
β	Change in exhaust area per change in inlet area	N.D.

The pneumatic positioning servo is most often referred to as the "hot gas servo," since a hot gas is often used as the working fluid. The following treatment is not restricted by the temperature of the gas and therefore applies to cold as well as hot gas systems.

Pneumatic systems usually derive their high-pressure working fluid from either a high-pressure storage bottle (cold gas) or a gas generator (hot gas). Figs. 28, 29, and 30 picture the three main configurations of pneumatic systems using hot and cold gas. In all three designs it is common practice to exhaust the working fluid overboard, since it is less costly to store a large quantity of high-pressure working fluid in the form of solid, liquid, or gas and exhaust it overboard than to include the plumbing and pumps necessary to repressurize and reuse the fluid.

In all these systems, the gas supply pressure downstream of the regulator may be considered constant. In addition, since the control valves have resonances well above the overall system bandwidth, one may ignore the higher-order valve dynamics.

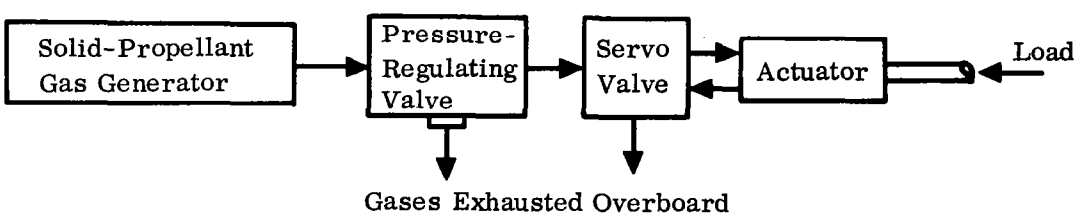

Figure 28. Solid Propellant Hot Gas System

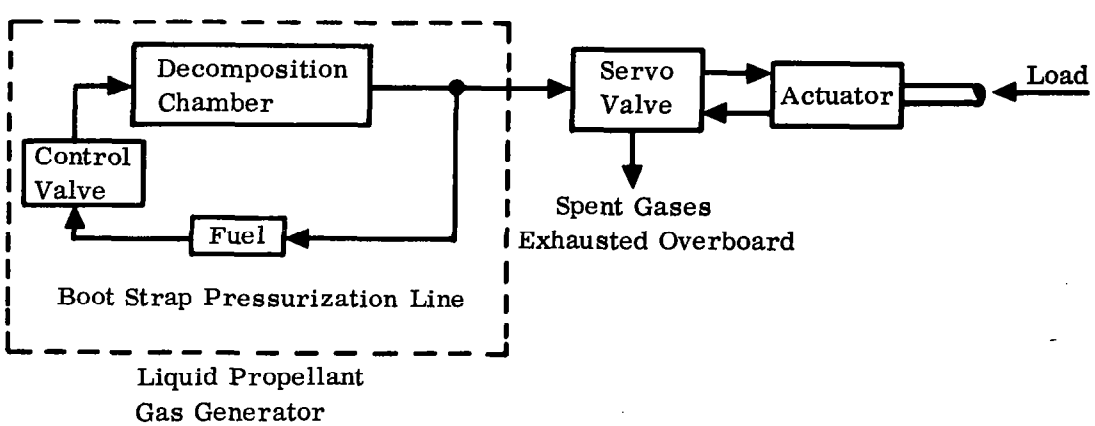

Figure 29. Liquid Propellant Hot Gas System

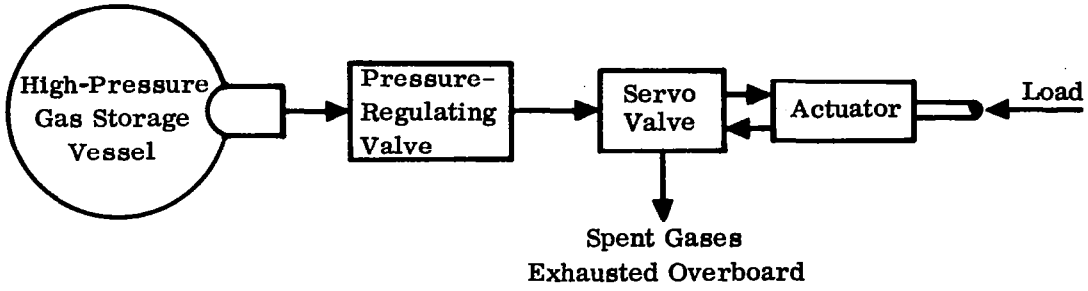

Figure 30. Stored Gas System

Four basic relationships are required in the analytic treatment of pneumatic servos:

a. Valve spool motion to valve current.

b. Orifice equation— gas flow versus orifice area and pressures.

c. Piston and cylinder relationship between volume changes, flow, and pressure.

d. Load pressure equations relating piston pressures to load response.

The first relationship is assumed a simple proportionality if the dynamics of the valve are neglected. By the nature of the gas laws, the second and third are nonlinear and require a small perturbation approach to provide reasonable linearization. The final relationship is well established by definition. Combined, these relationships lead to the transfer function (δ/i_v) of the servo actuator.

Pneumatic Orifice

The weight rate of flow of a gas through an orifice is described by

$$W = N \frac{A_h P_u}{\sqrt{T}} \tag{67}$$

where $N = N(P_d/P_u)$ is the nonlinear flow coefficient for a compressible fluid.

For subsonic flow,

$$\frac{P_d}{P_u} > r$$

and the coefficient is commonly given by

$$N = C_d\left(\frac{P_u}{P_d}\right)^{\frac{1}{\gamma}}\sqrt{\frac{2g}{R_g}\frac{\gamma}{\gamma-1}\left[1-\left(\frac{P_u}{P_d}\right)^{\frac{\gamma-1}{\gamma}}\right]} \tag{68}$$

For supersonic flow,

$$\frac{P_d}{P_u} \leq r$$

and

$$N = r$$

A simpler, more easily manageable expression that yields the same results for subsonic flow is given by

$$N = r\left[1-\left(\frac{1-r\frac{P_u}{P_d}}{1-\frac{P_u}{P_d}}\right)^2\right]^{\frac{1}{2}} \tag{69}$$

Eq. (67) can be linearized if it is assumed that the variables are limited to small excursions about their average values. Taking the differential of W,

$$dW = \frac{1}{\sqrt{T}}\left(A_h P_u dN + A_h N dP_u + P_u N dA_h\right) \tag{70}$$

where dN, as it appears, is not a useful variable and must be found in terms of P_d/P_u.

$$dN = \frac{\partial N}{\partial\left(\frac{P_d}{P_u}\right)}d\left(\frac{P_d}{P_u}\right) = \frac{\partial N}{\partial\left(\frac{P_d}{P_u}\right)}\left(\frac{P_u dP_d - P_d dP_u}{P_u^2}\right)$$

$$= -C\left(\frac{P_u dP_d - P_d dP_u}{P_u^2}\right) \tag{71}$$

Combining (70) and (71),

$$dW = \frac{A_h}{\sqrt{T}} \left[\left(C \frac{P_d}{P_u} + N \right) dP_u - (C)\, dP_d + \left(\frac{P_u N}{A_h} \right) dA_h \right] \tag{72}$$

which describes the change in the weight rate of gas flow through a sharp-edged orifice as a function of area and pressure variations.

Piston and Cylinder

The time differentiation of the equation of state, $PV = mg\, R_g T$, for a volume of gas yields

$$\frac{\dot{P}}{P} + \frac{\dot{V}}{V} = \frac{\dot{T}}{T} + \frac{R_g T}{PV} W \tag{73}$$

where $W = \frac{d(mg)}{dt}$

Assuming a polytropic process for the control volume in the cylinder, the pressure is related to the temperature by

$$\frac{P^{\left(\frac{n-1}{n}\right)}}{T} = \text{constant} \tag{74}$$

where n ranges from 1.0 for an isothermal process to γ for an adiabatic process. The time differentiation of (74) gives

$$\left(\frac{n-1}{n}\right) \frac{\dot{P}}{P} = \frac{\dot{T}}{T} \tag{75}$$

Substituting Eq. (75) in (73) to eliminate the temperature terms, a time-variable volume relationship is obtained as

$$W = \frac{1}{R_g T} \left[\left(\frac{1}{n} \right) V \dot{P} + P \dot{V} \right] \tag{76}$$

Taking the small perturbation approach as before, a linear approximation to Eq. (76) can be written by assuming the coefficients of the differential quantities to be average values over one cycle and denoting these values by the subscript $( )_o$.

$$W = \frac{1}{R_g T} \left[\left(\frac{1}{n} \right) V_o \dot{P} + P_o \dot{V} \right] \tag{77}$$

Since

$$\frac{dV}{dt} = A \frac{dx}{dt}$$

the weight rate of flow to both sides of the piston-cylinder combination can be described by

$$W_{1c} = \frac{1}{R_g T}\left[\left(\frac{1}{n}\right)V_{10}\dot{P}_1 + A_1 P_{10}\dot{x}\right] \tag{78}$$

$$W_{2c} = \frac{1}{R_g T}\left[\left(\frac{1}{n}\right)V_{20}\dot{P}_2 + A_2 P_{20}\dot{x}\right]$$

Combined Orifice, Valve, and Piston

An open-center (underlap) valve is assumed such that there is always a flow of gas through it* (Fig. 31). This type of valve is popular for vehicles with short mission times and is relatively easy to analyze. A closed-center valve with a small overlap will have the same type of linearized transfer function.

For simplicity, assume that both inlet and exhaust orifices are choked such that N = r. Then, neglecting the valve actuation dynamics,

$$W_v = f(Y, P)$$

where Y is the spool displacement, a function of input current.

Using Eq. (72), the effective flows from the valve can be written as

$$W_{1v} = \frac{r}{\sqrt{T}}\left[K_i\left(P_s + \beta P_{10}\right)i - Ae_{10}P_1\right] \tag{79}$$

$$W_{2v} = \frac{-r}{\sqrt{T}}\left[K_i\left(P_s + \beta P_{20}\right)i - Ae_{20}P_2\right]$$

*The weight rates of flow through the two sides of the system at a steady null position are given by

$$W_{o1} = \frac{rAe_{10}P_{10}}{\sqrt{T}} = \frac{rAi_{10}P_s}{\sqrt{T}}$$

$$W_{o2} = \frac{rAe_{20}P_{20}}{\sqrt{T}} = \frac{rAi_{20}P_s}{\sqrt{T}}$$

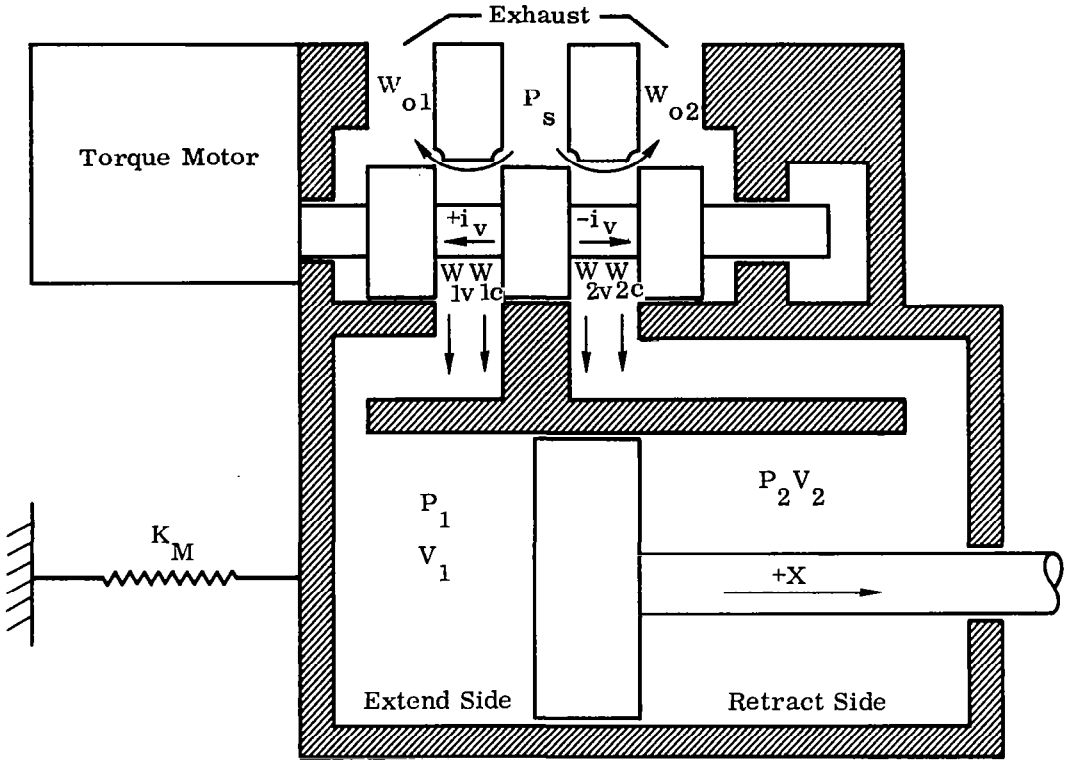

Figure 31. Pneumatic Positioning Servo with Open-Center Control Valve

Combining Eqs. (78) and (79) relates the actuator behavior to the valve input.

$$\frac{r}{\sqrt{T}} K_i \left(P_s + \beta P_{10}\right) i = \frac{A_1 P_{10}}{R_g T} \frac{dx}{dt} + \frac{r}{\sqrt{T}} Ae_{10} P_1 + \frac{V_{10}}{n R_g T} \frac{dP_1}{dt} \qquad (80)$$

$$\frac{-r}{\sqrt{T}} K_i \left(P_s + \beta P_{20}\right) i = \frac{-A_2 P_{20}}{R_g T} \frac{dx}{dt} + \frac{r}{\sqrt{T}} Ae_{20} P_2 + \frac{V_{20}}{n R_g T} \frac{dP_2}{dt}$$

It should be noted that numerous assumptions have been made in obtaining Eqs. (80). The temperature of the gas in the actuator may not be the same as the temperature of the valve, but this can be handled by modifying the value of average exhaust area or valve gain appropriately. Piston leakage or other considerations, such as stabilizing volumes, may be included in the equations by application of Eqs. (72) and (77).

The introduction of the following additional assumptions results in a considerably simplified final expression.

$$P_{10} = P_{20}$$

$$A_1 = A_2$$

$$Ae_{10} = Ae_{20}$$

$$V_{10} = V_{20}$$

Combining Eqs. (80) and incorporating the above results in a single expression for the valve and actuator,

$$\frac{2r}{\sqrt{T}} K_i \left(P_s + \beta P_{10}\right) i = \frac{2 A_1 P_{10}}{R_g T} \frac{dx}{dt} + \frac{r}{\sqrt{T}} Ae_{10} P_L + \frac{V_{10}}{n R_g T} \frac{dP_L}{dt} \tag{81}$$

Actuator Load Pressure

Assuming a balanced actuator and the linearizing condition of operation about steady-state operating points, the actuator load pressure is given by

$$A_1 P_L = \frac{1}{R}\left[K_R \delta + f(\dot{\delta})\, \dot{\delta} + I_R \ddot{\delta}\right] \tag{82}$$

(See Fig. 31.)

The friction term, $f(\dot{\delta})$, cannot be linearized for general inputs. However, its effects can be studied on computers or linearized for sinusoidal inputs by means of describing functions. (For more details on the latter, see Sec. 3.2.3.1.)

If the actuator mounting can be described as a simple spring, the load displacement differs from the piston displacement as follows.

$$x = R\delta + \frac{A_1 P_L}{K_M} \tag{83}$$

Combining Eqs. (82) and (83) gives:

$$K_M x = \left[K_M R + \frac{K_R}{R}\right]\delta + \frac{f(\dot{\delta})}{R}\dot{\delta} + \frac{I_R}{R}\ddot{\delta} \tag{84}$$

Combined Transfer Function

The transfer function from valve input to either actuator position or load position can now be obtained by combining Eqs. (81), (82), and (84). The resulting expression is somewhat complicated, and a better feel for the various terms can be obtained by investigating the special case:

$$f(\dot{\delta}) = K_r = 0$$

$$K_M = \infty$$

The resulting expression gives the transfer function from valve input to load displacement of the open-loop servo.

$$\frac{\delta(s)}{i(s)} = \frac{\dfrac{R_g r K_i \sqrt{T}\left[P_s + \beta P_{10}\right]}{A_1 P_{10} R}}{s\left[\dfrac{V_{10} I_R}{2nA_1^2 R^2 P_{10}} s^2 + \dfrac{Ae_{10} r I_R R_g \sqrt{T}}{2P_{10} R^2 A_1^2} s + 1\right]} \tag{85}$$

Eq. (85) indicates a number of basic facts concerning gas servo behavior:

a. The open-loop gain is proportional to the square root of the absolute temperature.

b. The open-loop natural frequency is not a function of temperature.

c. Some damping is available as a result of the average exhaust area, but this damping is temperature-dependent.

The most common form of gas servo has fixed inlet orifices and variable exhaust orifices. Eq. (85) is not directly applicable to such a valving configuration without a few minor changes. The modification consists of redefining βK_i in terms of the exhaust orifice only and allowing β to approach infinity while K_i approaches zero and the value of βK_i is held constant. The net result is that the supply pressure drops out of the expression for gain.

For most applications in a closed-loop position servo, the open-loop natural frequency is not sufficiently high with respect to control frequencies that it can be ignored. Some form of the derivative of position is required in the feedback for damping. The

resulting closed-loop transfer function will be at least third-order and probably of even higher order; the principal behavior can be adequately described with a second-order equation. In the absence of more detailed information, a second-order system with a natural frequency equal to the open-loop natural frequency and a damping factor of 0.3 to 0.5 may be used. For a more detailed treatment of the subject see Ref. 15.

3.2.3 Hydraulic Actuators

Hydraulic systems offer a number of advantages over both electrical and pneumatic types. They have greater power-carrying capability and can deliver much larger torques than electrical equipment of comparable size and weight. For continuous operation, they offer a minimum equipment/horsepower ratio. Where intermittent operation is required, a hydraulic system can provide large amounts of power from a small-volume accumulator. Their dynamic characteristics are expressed by small time constants; they develop much higher peak T^2/I (torque, inertia) ratios than electrical motors of the same peak power. These attributes, among others, have contributed to the wide acceptance of hydraulic systems to fulfill the control actuation requirements of launch vehicles.

The most common form of utilization in vehicle control loops consists of a high-pressure supply (pump), an electrohydraulic servovalve, a hydraulic actuator (cylinder), a feedback transducer, and a servoamplifier. Many systems presently in use also include an accumulator, which acts as a hydraulic capacitor in the system.

The hydraulic power supplies currently used are of two main types. One employs a variable displacement pump whose flow output is controlled by means of a servo sensing the high-pressure side of the hydraulic system. A relief valve is also connected from the high-pressure side to the low-pressure side (hydraulic reservoir) of the system to minimize pressure transients above the operating pressures of the system. For normal operation, the relief valve remains closed, opening only when pressures exceed a value overcoming the preload on the relief valve. The second type uses a fixed-displacement pump with a relief valve to maintain the supply pressure within set limits as well as to meet the normal flow requirements. In this system the relief valve is normally open such that supply pressure and valve opening, which is dependent on supply pressure, maintain flow through the relief valve equal to the flow output of the fixed-displacement pump. When there is a flow demand the relief valve closes and the supply pressure is therefore reduced.

The dynamics of both power supply and relief valve will be discounted in the ensuing discussion. Both normally exhibit a fairly flat response with minimal phase shift within the bandwidths of overall control servo loops. This being the case, supply pressure will be assumed constant at the value of zero flow demand.

Electrohydraulic valves are usually designed for flow control or pressure control, or a combination of the two. A difficulty in assigning linear transfer functions to represent servovalve response is that these units are highly complex devices that exhibit high-order, nonlinear responses. Still, representation is necessary only in the frequency range of interest and this can usually be done by first- or second-order approximations. Ref. 13 gives transfer functions for some standard valves. These vary from a simple lag, as a good low-frequency approximation for a flow control valve, to more complex representations for other types. The model, of course, can be further approximated by a simple gain for applications below the valve corner frequency.

Stability analyses of electrohydraulic control systems based on linear transfer functions can be only qualitatively correct for systems that are inherently nonlinear. Such analyses merely indicate the results that would be obtained if the system were linear and therefore have no real quantitative significance. The following derivations are intended to illustrate how the form of the linear representation of an actuating system can be used to describe the nonlinear model. The method is due to Backus[3]; its results have been successfully employed on existing vehicles.

3.2.3.1 Electrohydraulic Position Servo

The following definitions and symbols are used in this section.

A	Effective piston area	ft^2
B	Bulk modulus of hydraulic fluid	lb/ft^2
C_V	Viscous friction coefficient	ft-lb/rad/sec
C_B	Coulomb friction coefficient	ft-lb
$\bar{C}_f$	Equivalent admittance for gimbal friction	ft-lb/rad/sec
C_L	Discharge coefficient for leakage bypass orifice	$ft^3/sec/\sqrt{lb/ft^2}$
$\bar{C}_L$	Equivalent admittance for $\bar{C}_L$	
δ_c	Input command to servoamplifier	rad
δ	Engine deflection (gimbal angle)	rad
δ_F	Feedback signal to servoamplifier	rad
g_E	In-phase component of equivalent admittance	
G_{NL}	Equivalent admittance for nonlinear element	
i_v	Current in servovalve coil	ma
I_R	Moment of inertia of engine about swivel point	$sl-ft^2$
K_a'	Servoamplifier gain	ma/volt

K_c	No-load open-loop velocity gain	rad/sec/rad
$\bar{K}_c$	Effective (at load) open-loop velocity gain	rad/sec/rad
K_c'	Effective (at load) open-loop velocity gain (under low load pressure assumption)	rad/sec/rad
K_F	Feedback transducer gain	volts/foot
K_{mp}	Spring constant of mount	lb/ft
K_{mc}	Spring constant of piston rod	lb/ft
K_v	Valve flow gain	$(ft^3/sec)/ma\sqrt{lb/ft^2}$
K_1	Valve input displacement gain	ft/ma
K_2	Proportionality constant	$(ft^3/sec)/ft\sqrt{lb/ft^2}$
ℓ_a	Orifice leakage coefficient	$(ft^3/sec)/(lb/ft^2)$
ℓ_v	Spool leakage coefficient	$(ft^3/sec)/(lb/ft^2)$
P_L	Pressure differential across piston	lb/ft^2
P_S	Supply pressure to valve	lb/ft^2
P_R	Reservoir or exhaust pressure	lb/ft^2
Q_v	Fluid flow rate	ft^3/sec
R	Moment arm of the actuator about the engine gimbal point	ft
T_f	Frictional torque at gimbal	ft-lb
T_L	Load torque	ft-lb
V_C	Control signal to valve	volts
V_E	Error signal	volts
V_F	Feedback signal	volts
V_T	Total volume of fluid under compression	ft^3
x_c	Cylinder mount displacement	ft
x_p	Piston rod displacement	ft
x_v	Valve spool displacement	ft

$$V_C = R K_F \delta_c \tag{86}$$

$$V_F = K_F\left(x_p - x_c\right) \tag{87}$$

$$V_E = V_C - V_F \tag{88}$$

The electrohydraulic servo used to gimbal engines for control through thrust-vectoring is a highly nonlinear device. Fig. 32 is a simplified block diagram of such a system used as a position servo.

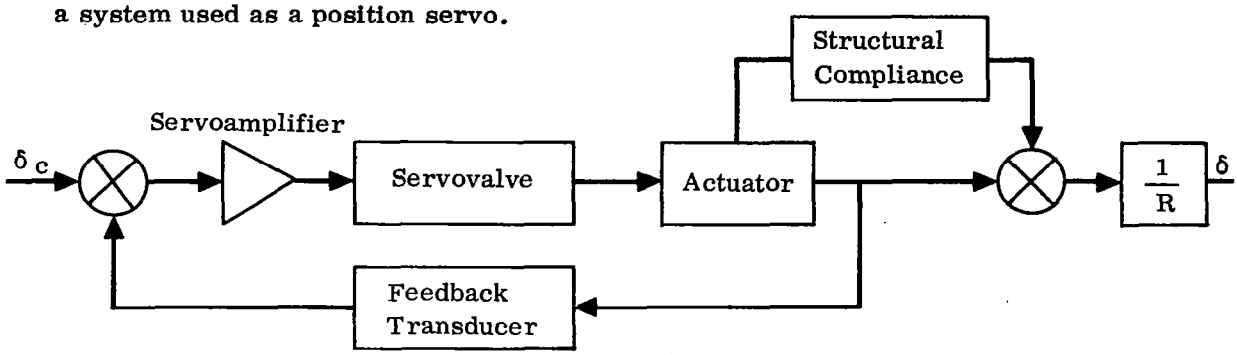

Figure 32. Block Diagram of Thrust Vector Servo

The servoamplifier can be assumed to be linear, as can the feedback transducer, since both are usually designed so that their saturation limits are above those of either the flow limit or actuator stop. The servovalve is a flow-control type coupled to an actuator having a leakage orifice across the load piston to provide damping. The output piston rod is hinged to a rocket engine that moves about its gimbal point (Fig. 33). The transducer feeds back the motion of the rod to the servoamplifier.

We can assume that the flow from the servovalve into one side of the actuating cylinder is equal to the flow out of the other side. For relatively low load pressures, this flow of hydraulic fluid, Q_V, from the servovalve is given by

$$Q_V = K_2 x_v \sqrt{P_S - P_R} - \ell_v P_L \tag{89}$$

where $\ell_V P_L$ represents the leakage across the spool and K_2 is proportional to a discharge coefficient that may vary with both the spool displacement and the actuator load pressure. The present derivation assumes a constant value.

The total flow to the cylinder is the sum of the piston displacement flow, leakage flow, and compressibility flow, such that

$$Q_v = A\left(\dot{x}_p - \dot{x}_c\right) + \ell_a P_L + \frac{V_T}{4B}\dot{P}_L \tag{90}$$

The actuator load pressure depends on the dynamic equilibrium of the control system. Assuming that the system damping and spring rate are provided by the load torques and friction torque,

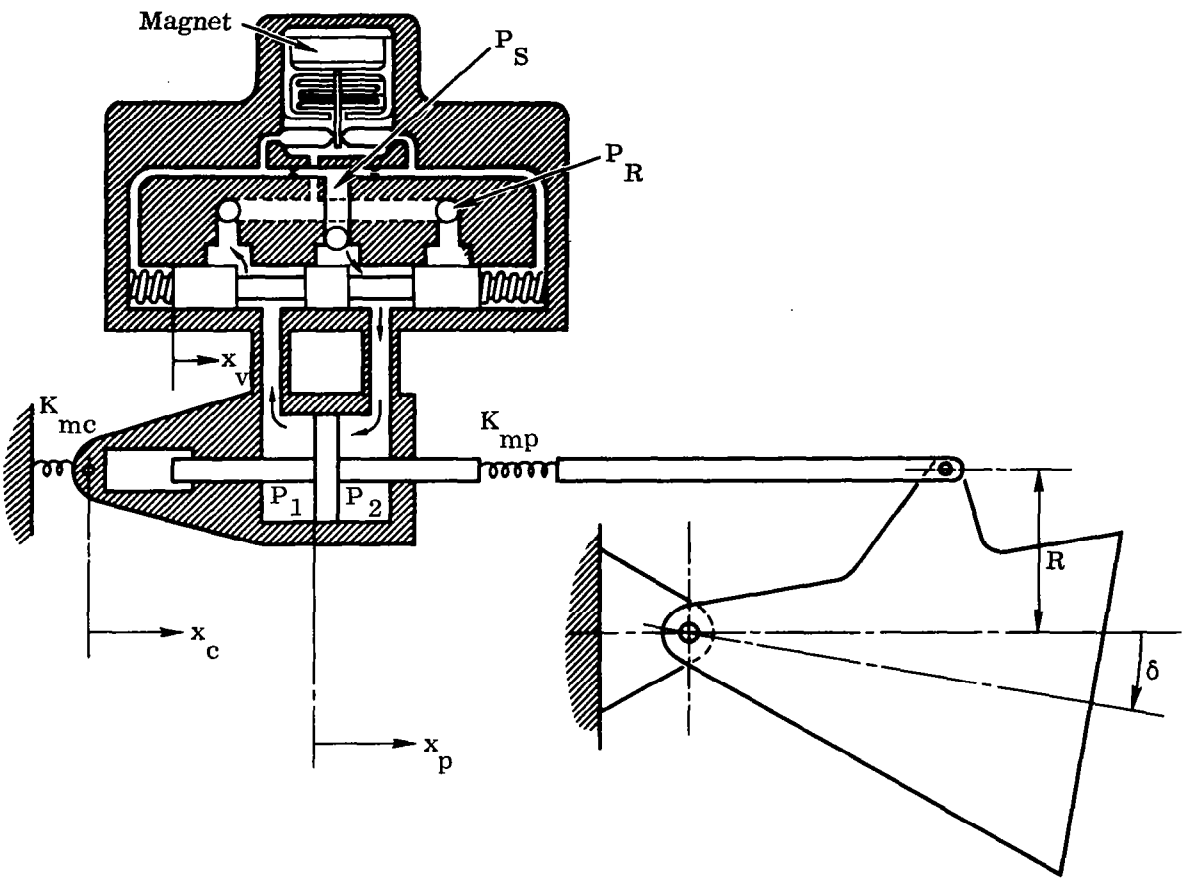

Figure 33. Schematic of Electrohydraulic Servo System

$$I_R \ddot{\delta} + T_L' = R \left(A P_L \right) \tag{91}$$

where

$$T_L = T_L + T_f$$

The torque, T_L, consists of all inertial load torques due to the accelerations of the various body modes, rigid and elastic. T_f is the torque due to gimbal friction and can be expressed as a combination of viscous (C_V) and coulomb (C_B) friction.

$$T_f = C_V \dot{\delta} + C_B \operatorname{sgn} \dot{\delta} \tag{92}$$

The load pressure, P_L, displaces the piston rod and engine. With respect to the cylinder, this displacement is obtained from

$$A P_L = K_{mp} \left(x_p - R \delta \right) \tag{93}$$

The displacement of the cylinder relative to the vehicle structure is obtained from

$$A P_L = -K_{mc} \dot{x}_c \tag{94}$$

Substituting (93) and (94) in (90) and then combining with (89) yields

$$\left[\frac{V_T}{4B} + A^2\left(\frac{1}{K_{mp}} + \frac{1}{K_{mc}}\right)\right]\dot{P}_L + \left(\ell_a + \ell_v\right) P_L = K_2 x_v \sqrt{P_S - P_R} - A R \dot{\delta} \tag{95}$$

The spool displacement x_v, is proportional to the valve current.

$$x_v = K_1 i_v \tag{96}$$

Given a linear amplifier, K_a'

$$x_v = K_1 K_a' V_E \tag{97}$$

$$= K_1 K_a' \left(V_C - V_F\right) \tag{98}$$

Introducing (86) and (87) in (98) and substituting (93) and (94) in the resulting expression, the valve displacement can be written as

$$x_v = K_1 K_a' K_F \left[R\left(\delta_c - \delta\right) - A\left(\frac{1}{K_{mp}} + \frac{1}{K_{mc}}\right) P_L\right] \tag{99}$$

Combining (95) and (99),

$$\left[\frac{V_T}{4B} + A^2\left(\frac{1}{K_{mp}} + \frac{1}{K_{mc}}\right)\right]\dot{P}_L + \left[\ell_a + \ell_v + K_a' K_v K_F A\left(\frac{1}{K_{mp}} + \frac{1}{K_{mc}}\right)\right] P_L$$

$$= K_a' K_v K_F R\left(\delta_c - \delta\right) - A R \dot{\delta} \tag{100}$$

where $K_v = K_1 K_2$, the valve flow gain parameter.

After substituting this in Eq. (91) and simplifying, we obtain, in Laplace notation,

$$\left\{I_R\left[\frac{V_T}{4B} + A^2\left(\frac{1}{K_{mp}} + \frac{1}{K_{mc}}\right)\right] s^3 + I_R\left[\ell_a + \ell_v + K_c A^2\left(\frac{1}{K_{mp}} + \frac{1}{K_{mc}}\right)\right] s^2 + A^2 R^2 s + A^2 R^2 K_c\right\}\delta = A^2 R^2 K_c \delta_c - \left\{\left[\frac{V_T}{4B} + A^2\left(\frac{1}{K_{mp}} + \frac{1}{K_{mc}}\right)\right] s + \left[\ell_a + \ell_v + K_c A^2\left(\frac{1}{K_{mp}} + \frac{1}{K_{mc}}\right)\right]\right\} T_L' \tag{101}$$

(The equivalent block diagram is shown in Fig. 34.)

This may be reduced to

$$\left[s^3 + 2\zeta_c\omega_c s^2 + \omega_c^2 s + K_c\omega_c^2\right]\delta = K_c\omega_c^2\delta_c - \frac{1}{I_R}\left(s + 2\zeta_c\omega_c\right)T_L' \quad (102)$$

or

$$\left[s\left(\frac{s^2}{\omega_c^2} + \frac{2\zeta_c}{\omega_c}s + 1\right) + K_c\right]\delta = K_c\delta_c - \frac{2\zeta_c}{I_R\omega_c}\left(\frac{s}{2\zeta_c\omega_c} + 1\right)T_L' \quad (103)$$

where

$$\left.\begin{aligned}
K_c &= \frac{K_a' K_F K_v \sqrt{P_S - P_R}}{A} \\
\omega_c^2 &= \left(\frac{1}{\omega_a^2} + \frac{1}{\omega_p^2} + \frac{1}{\omega_m^2}\right)^{-1} \\
\omega_a^2 &= \frac{4BA^2R^2}{I_R V_T} \\
\omega_p^2 &= \frac{R^2}{I_R}K_{mp} \\
\omega_m^2 &= \frac{R^2}{I_R}K_{mc} \\
\zeta_c &= \left[\frac{I_R\left(\ell_a + \ell_v\right)}{2A^2R^2} + \frac{K_c}{2\omega_c^2\left(1 + \frac{\omega_T^2}{\omega_a^2}\right)}\right]\omega_c \\
\frac{1}{\omega_T^2} &= \frac{1}{\omega_p^2} + \frac{1}{\omega_m^2}
\end{aligned}\right\} \quad (103a)$$

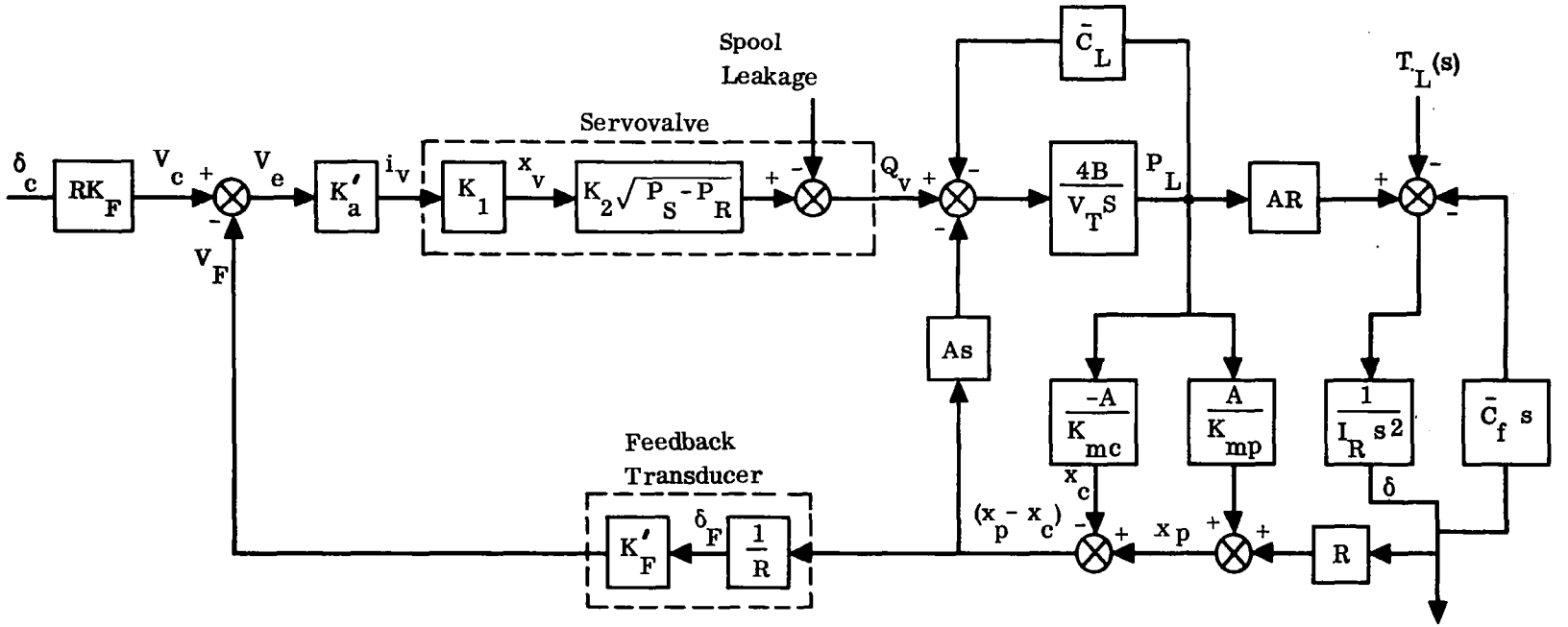

Figure 34. Block Diagram of Electrohydraulic Swivelled Rocket Engine Position Servo

The accounting of structural compliance and fluid compressibility in body bending computations, or the neglect of these effects for low-frequency applications, leads to

$$\omega_c \rightarrow \infty$$

which results in the simplification of Eq. (103) to a first-order expression.

If the mount and rod compliance ($1/K_m$) is included in the vehicle flexibility when the body bending modes are computed, this compliance correction is expressed as a function of the modal coordinates instead of the load pressure. In this case, or if the compliance is otherwise neglected,

$$\omega_T \rightarrow \infty$$

and parameters ω_c and ζ_c of Eqs. (102) and (103) reduce to

$$\left.\begin{aligned} \omega_c &= \omega_a \\ \zeta_c &= \left(\ell_a + \ell_v\right)\sqrt{\frac{B I_R}{A^2 R^2 V_T}} \end{aligned}\right\} \quad (104)$$

If the fluid compressibility is either neglected or accounted for in the body bending modes, then the term is omitted from Eq. (90) by setting

$$B \rightarrow \infty$$

Therefore,

$$\omega_a \rightarrow \infty$$

and Eq. (103) reduces to

$$\frac{\delta}{\delta_c} = \frac{K_c}{s + K_c} \quad (105)$$

Thus a set of simultaneous linear and nonlinear equations has been assembled into a linear expression, Eq. (103), and simplified to Eq. (105). In some cases, these may serve as first approximations to the system but will prove rather difficult to solve analytically when all the terms are correctly represented. Significant nonlinearities may occur in the valve gain, K_v, which is a function of valve current and hydraulic pressures; in the half-power flow functions of hydraulic pressure; in the piston orifice flow; and in the gimbal bearing friction. However, the above equations

may be used if equivalent linear terms can be found to describe the nonlinear functions.

The assumptions that justify a describing function analysis are well met in the elastic coupling study application; i.e., the signals are almost "purely harmonic," and frequencies other than the fundamental are greatly attenuated. These conclusions follow because the significant modal roots are very lightly damped and enjoy a suitable frequency separation,and the various modes are weakly coupled.

In Eq. (89), in combination with (98), linearization is implied in that K_v and ℓ_v are assumed constant. This is a good approximation for many commercial flow-compensated valves and can be further justified (if K_v should vary somewhat) by assuming a mean value for a range of operating conditions. Of course, a more elaborate valve flow model could be used to remove the restrictions (small amplitude at the higher frequencies), due to the low load-pressure approximation.

Removing this approximation, the valve flow can be described more generally by

$$Q_v = i_v K_v \sqrt{|P_S - P_R + P_L \operatorname{sgn} i_v|}\, \operatorname{sgn}(P_S - P_R + P_L \operatorname{sgn} i_v) \tag{106}$$

where K_v can be derived empirically as a function of P_L and i_v. The resulting function would include the leakage across the spool. In the following treatment, it will be assumed that the valve flow is parabolic and that K_v is a function of only P_L.

In Eq. (90), the leakage coefficient, ℓ_a, was used as a linear proportionality constant under the assumption of either laminar flow or very small perturbations about nominal. A more general definition of the leakage orifice flow is given by

$$C_L \sqrt{|P_L|}\ \operatorname{sgn} P_L$$

and Eq. (90) can be rewritten

$$Q_v = A\left(\dot{x}_p - \dot{x}_c\right) + C_L \sqrt{|P_L|}\ \operatorname{sgn} P_L + \frac{V_T}{4B}\dot{P}_L \tag{107}$$

The nonlinear equations, (91), (106), and (107), may be linearized as follows.

$$A\left(\dot{x}_p - \dot{x}_c\right) + \bar{C}_L P_L + \frac{V_T}{4B}\dot{P}_L = i_v K_v \sqrt{P_S - P_R + P_L} \tag{108}$$

$$I_R \ddot{\delta} + T_L + \bar{C}_f \dot{\delta} = R\left(A P_L\right) \tag{109}$$

where $\bar{C}_f \dot{\delta} = T_f$

$\bar{C}_L$ = the equivalent admittance for the leakage orifice discharge parameter

$\bar{C}_f$ = the equivalent admittance for the gimbal friction

and $\bar{C}_L$ and $\bar{C}_f$ are both amplitude- and frequency-dependent.

a. Equivalent Admittance

Assume the input signal to a nonlinear element to be

$$x_1 = a_1 \sin \omega t$$

The output signal from the nonlinear element would be periodic and may be expressed as a Fourier series in the form

$$x_2 = \sum_n A_n \sin n \omega t + \sum_n B_n \cos n \omega t$$

The coefficients of the fundamental components are

$$A_1 = \frac{1}{\pi} \int_{-\pi}^{\pi} x_2 \sin \omega t \, d(\omega t)$$

$$B_1 = \frac{1}{\pi} \int_{-\pi}^{\pi} x_2 \cos \omega t \, d(\omega t)$$

By definition, the equivalent admittance (nonlinear gain) is

$$G_{NL} = \frac{x_2}{x_1}$$ where all but the fundamental frequency components are omitted for the output function.

$$G_{NL} = \frac{A_1 \sin \omega t + B_1 \cos \omega t}{a_1 \sin \omega t}$$

$$= \frac{1}{a_1} \left(A_1 + j \, B_1 \right)$$

Since the motion is quasi-harmonic, $j = s/\omega$, and

$$G_{NL} = g_E + \frac{b_E}{\omega} s$$

where

$$g_E = \frac{A_1}{a_1} = \frac{1}{\pi a_1} \int_{-\pi}^{\pi} x_2 \sin \omega t \, d(\omega t) \tag{110}$$

$$b_E = \frac{B_1}{a_1} = \frac{1}{\pi a_1} \int_{-\pi}^{\pi} x_2 \cos \omega t \, d(\omega t) \tag{111}$$

Applying the results to the actuator load torque due to gimbal friction, the object is to determine what linear coefficient, $\bar{C}_f$, should be used, at a particular amplitude and frequency, in the linearization of Eq. (92) as represented in Eq. (109).

$$\frac{T_f}{\dot{\delta}} = \bar{C}_f = G_{NL}$$

Assume

$$\dot{\delta} = \bar{\dot{\delta}} \sin \omega t$$

where

$\bar{\dot{\delta}}$ is the input amplitude

Then

$$g_E = \frac{1}{\pi \bar{\dot{\delta}}} \int_{-\pi}^{\pi} T_f \sin \omega t \, d(\omega t)$$

$$= \frac{1}{\pi \bar{\dot{\delta}}} \int_{-\pi}^{\pi} \left(C_V \dot{\delta} + C_B \frac{\dot{\delta}}{|\dot{\delta}|} \right) \sin \omega t \, d(\omega t)$$

$$= \frac{2}{\pi} \int_0^{\pi} \left(C_V + \frac{C_B}{\bar{\delta} \, |\sin \omega t|} \right) \sin^2 \omega t \, d(\omega t)$$

$$= C_V + \frac{4}{\pi} \frac{C_B}{\omega \bar{\delta}}$$

and

$$b_E = 0$$

Therefore,

$$\bar{C}_f = C_V + \frac{4}{\pi} \frac{C_B}{\omega \bar{\delta}} \tag{112}$$

For the leakage orifice flow, we assume

$$P_L = \bar{P}_L \sin \omega t$$

$$g_E = \frac{1}{\pi \bar{P}_L} \int_{-\pi}^{\pi} \left(C_L \sqrt{|P_L|} \frac{P_L}{|P_L|} \right) \sin \omega t \, d(\omega t)$$

$$= \frac{2 C_L}{\pi \bar{P}_L} \int_0^{\pi} \sin^{3/2} \omega t \, d(\omega t)$$

$$= \frac{1.11 C_L}{\sqrt{\bar{P}_L}}$$

and

$$b_E = 0$$

Therefore,

$$\bar{C}_L = \frac{1.11 C_L}{\sqrt{\bar{P}_L}} \tag{113}$$

b. Effective Servovalve Velocity Gain

Rewriting Eq. (106),

$$\frac{Q_v}{i_v} = K_v \sqrt{P_S - P_R} \left[\sqrt{1 + \frac{P_L}{P_S - P_R}} \right] \tag{114}$$

and assuming that the load pressure $P_L < (P_S - P_R)$, the last term can be expanded as a power series.

$$\frac{Q_v}{i_v} = K_v\sqrt{P_S - P_R}\left[1 + \frac{1}{2}\left(\frac{P_L}{P_S - P_R}\right) - \frac{1}{8}\left(\frac{P_L}{P_S - P_R}\right)^2 \cdots\right] \tag{115}$$

Let

$$\left.\begin{aligned} i_v &= \bar{i}_v \sin(\omega t) \\ P_L &= \bar{P}_L \sin(\omega t - \phi) \end{aligned}\right\} \tag{116}$$

where ϕ is the phase angle (assumed lagging) of P_L with respect to i_v.

The equivalent admittance for the servovalve flow is defined by

$$g_E = \frac{1}{\pi \bar{i}_v}\int_{-\pi}^{\pi} Q_v \sin \omega t \, d(\omega t)$$

Using only the first two terms of the expansion,

$$g_E = \frac{K_v\sqrt{P_S - P_R}}{\pi \bar{i}_v}\int_{-\pi}^{\pi} i_v\left[1 + \frac{1}{2}\left(\frac{P_L}{P_S - P_R}\right)\right]\sin \omega t \, d(\omega t)$$

Substituting (116) into the above and integrating,

$$g_E = K_v\sqrt{P_S - P_R}\left[1 + \frac{4}{3\pi}\left(\frac{\bar{P}_L}{P_S - P_R}\right)\cos\phi\right] \tag{117}$$

The reactive transmission of the equivalent admittance, b_E, is not zero. However its effect has been found negligible for most practical purposes.

Introducing (117) into (108) yields

$$A\left(\dot{x}_p - \dot{x}_c\right) + \bar{C}_L P_L + \frac{V_T}{4B}\dot{P}_L = i_v K_v \alpha \sqrt{P_S - P_R} \tag{118}$$

where

$$\alpha = 1 + \frac{4}{3\pi}\left(\frac{\bar{P}_L}{P_S - P_R}\right)\cos\phi$$

Since the velocity gain

$$K_c = K_a' K_F K_v \sqrt{P_S - P_R}$$

Eq. (118) leads us to define an effective velocity gain as

$$\bar{K}_c = \alpha K_c \tag{119}$$

where K_c is amplitude- and frequency-dependent.

Solving and rearranging as before, we obtain the following equivalent linear transfer function:

$$\left\{I_R\left[\frac{V_T}{4B} + \frac{A^2}{K_m}\right]s^3 + I_R\left[\bar{C}_L + \bar{K}_c\,\frac{A^2}{K_m} + \frac{\bar{C}_f}{I_R}\left(\frac{V_T}{4B} + \frac{A^2}{K_m}\right)\right]s^2 + \left[A^2R^2 + \bar{C}_f\left(\bar{C}_L + \bar{K}_c\,\frac{A^2}{K_m}\right)\right]s + A^2R^2\bar{K}_c\right\}\delta$$

$$= A^2R^2\bar{K}_c\,\delta_c - \left[\left(\frac{V_T}{4B} + \frac{A^2}{K_m}\right)s + \left(\bar{C}_L + \bar{K}_c\,\frac{A^2}{K_m}\right)\right]T_L \tag{120}$$

where

$$\frac{1}{K_m} = \frac{1}{K_{mp}} + \frac{1}{K_{mc}}$$

This, in turn, can be reduced to

$$\left[s^3 + 2\zeta_{cn}\omega_{cn}s^2 + \omega_{cn}^2 s + \bar{K}_c\,\omega_c^2\right]\delta = \bar{K}_c\,\omega_c^2\,\delta_c - \frac{1}{I_R}\left(s + \bar{K}_o\right)T_L \tag{121}$$

where

$$K_o = \frac{\bar{C}_L + \bar{K}_c \frac{A^2}{K_m}}{\frac{V_T}{4B} + \frac{A^2}{K_m}}$$

$$\omega_c^2 = \frac{(AR)^2}{I_R\left[\frac{V_T}{4B} + \frac{A^2}{K_m}\right]} \qquad \text{(same as in 103a)}$$

$$\omega_{cn}^2 = \omega_c^2 + \frac{\bar{C}_f}{I_R}\bar{K}_o$$

$$2\zeta_{cn}\omega_{cn} = \bar{K}_o + \frac{\bar{C}_f}{I_R}$$

$$\frac{\omega_{cn}^2}{\omega_c^2} = 1 + \frac{\bar{C}_f \bar{K}_o}{I_R \omega_c^2}$$

} (121a)

Dividing through by ω_c^2 yields

$$\left[s\left(\frac{s^2}{\omega_c^2} + \frac{2\zeta_{cn}\omega_{cn}}{\omega_c^2}\, s + \left[1 + \frac{\bar{K}_o \bar{C}_f}{I_R \omega_c^2}\right]\right) + \bar{K}_c\right]\delta$$

$$= \bar{K}_c \delta_c - \frac{1}{I_R \omega_c^2}\left(s + \bar{K}_o\right) T_L \qquad (122)$$

For purposes of low-frequency stability studies, fluid compressibility as well as mount and rod compliance can be neglected, leading to

$$\omega_c \to \infty$$

and Eq. (122) can be approximated by

$$\frac{\delta}{\delta_c} = \frac{\bar{K}_c}{s + \bar{K}_c} \tag{123}$$

Suppose we wish to retain the following assumptions:

1. Low load pressures, $P_L \ll (P_S - P_R)$.
2. Negligible leakage across the valve spool.
3. K_v a constant independent of P_L and i_v.

Then we simply let $\alpha = 1$ in Eq. (119) and apply the results to (120). After rearranging, we obtain

$$\left\{\frac{s^3}{\omega_c^2} + \left(\frac{K_o + \bar{C}_f/I_R}{\omega_c^2}\right) s^2 + \left[1 + \frac{\bar{C}_f}{(AR)^2}\left(\bar{C}_L + K_c \frac{A^2}{K_m}\right)\right] s + K_c\right\} \delta$$

$$= K_c \delta_c - \left[\frac{s}{I_R \omega_c^2} + \frac{1}{(AR)^2}\left(\bar{C}_L + K_c \frac{A^2}{K_m}\right)\right] T_L \tag{124}$$

where now

$$K_o = \frac{\bar{C}_L + K_c \dfrac{A^2}{K_m}}{\dfrac{V_T}{4B} + \dfrac{A^2}{K_m}}$$

In the low-frequency range, Eq. (124) may be simplified by letting $\omega_c \to \infty$, and $T_L \to 0$. Then we have

$$\frac{\delta}{\delta_c} = \frac{K_c'}{s + K_c'} \tag{125}$$

where

$$K_c' = K_c \left[1 + \frac{\bar{C}_f}{(AR)^2}\left(\bar{C}_L + K_c \frac{A^2}{K_m}\right)\right]^{-1}$$

The equivalent linear transfer functions (121), (123), etc., are true only for $s = j\omega$, although they can be sufficiently accurate for small-valued σ in $s = \sigma + j\omega$. Therefore they can also be said to be approximately valid in the vicinity of the $(j\omega)$-axis.

The mathematical expedient of letting ω_c approach infinity implies that $K_m \to \infty$. However, the term involving K_m appears in the definition of K_c' above, by which it is implied that a finite (though large) value of K_m is still a first-order effect for low-frequency studies. This is a property of the particular system (with given numerical values), and the validity of this approximation must be verified for each individual system studied.

c. Determination of Equivalent Admittance

The equivalent admittances determined in the foregoing require a knowledge of ω, $\bar{\delta}$, $\bar{P}_L$, and ϕ for their numerical calculations. First the amplitude $(\bar{\delta})$ and the frequency (ω) of the output is specified. This permits calculation of $\bar{C}_f$, Eq. (112). Next, assume that the output load torque, T_L, is either zero or of minor importance in determining the amplitude of actuator load pressure. This restriction can be eliminated in digital routines, utilizing frequency-response or root-locus techniques, by employing an iterative procedure.

From Eq. (109),

$$P_L(j\omega) = -\frac{1}{AR}\left(I_R\,\omega^2 - \bar{C}_f\, j\omega\right)\delta(j\omega)$$

Hence

$$\left.\begin{aligned} \bar{P}_L &= -\frac{\bar{\delta}}{AR}\left[\left(I_R\,\omega^2\right)^2 + \left(\bar{C}_f\,\omega\right)^2\right]^{1/2} \\ \text{and} \\ \phi &= \tan^{-1}\left(\frac{-\bar{C}_f}{I_R\,\omega}\right) \end{aligned}\right\} \quad (126)$$

For given values of the system parameters, a chart showing $\bar{K}_c$ or K_c' as a function of $\bar{\delta}$ and ω can be constructed. Each set of curves is for particular values of actuator parameters and will change as these parameters are varied. (See Figs. 35 and 36.)

Finally, note that in computing these coefficients, the amplitude $(\bar{\delta})$ used must be the <u>total</u> angle, since this is the angle through which the bearing friction couple acts.

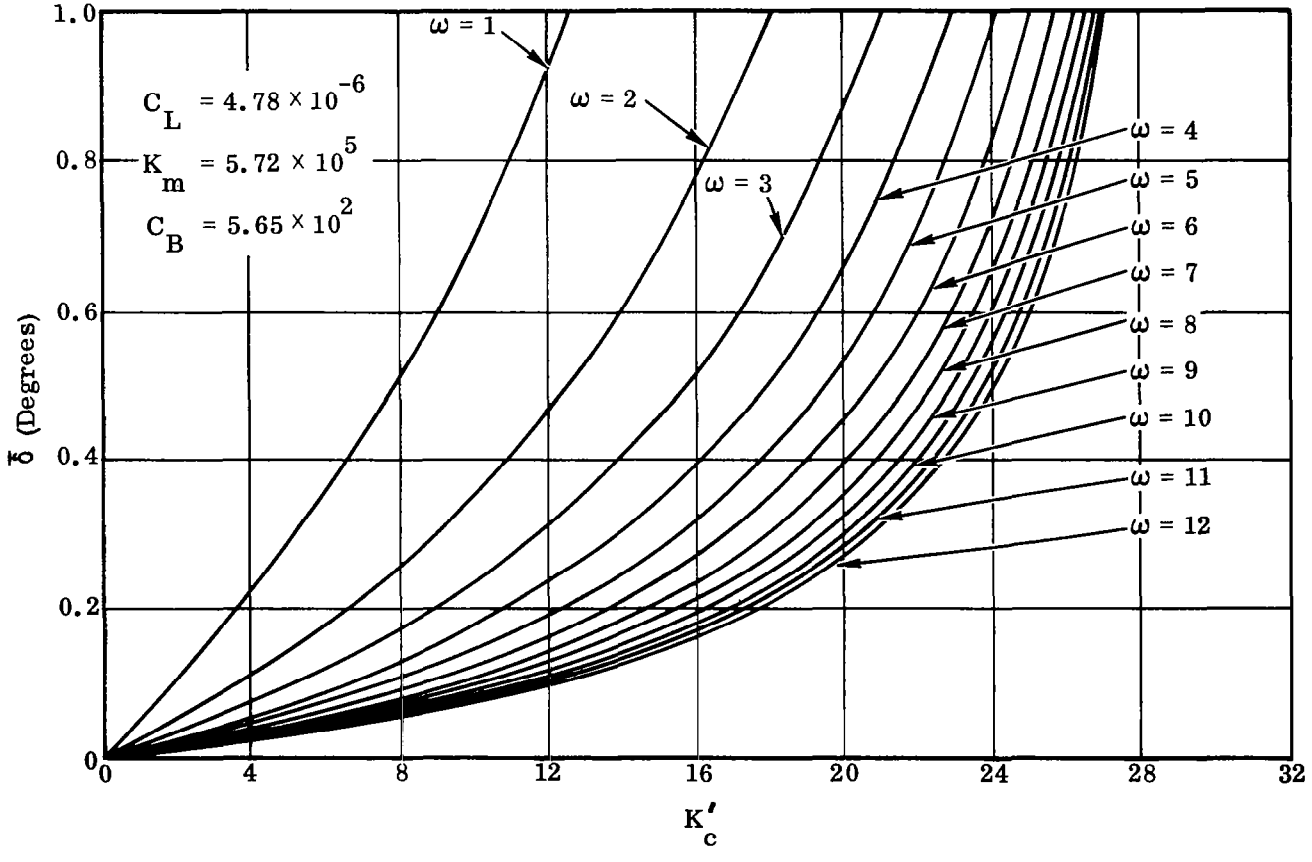

Figure 35. Low-Frequency Approximation, $K_c'/(s + K_c')$; Example 1

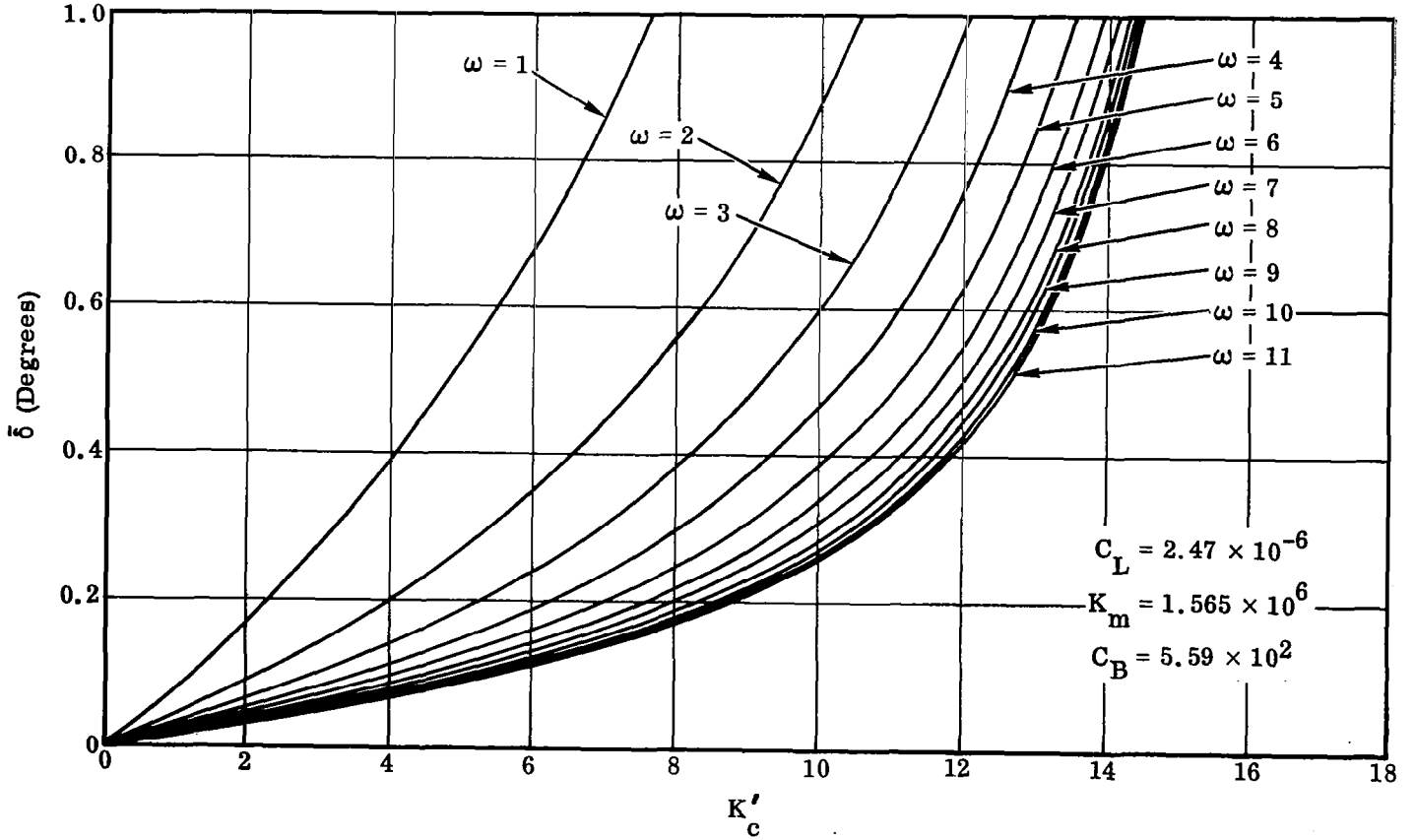

Figure 36. Low-Frequency Approximation, $K_c'/(s + K_c')$; Example 2

It is also the angle whose acceleration is related to load pressure, P_L, in computing the leakage and other valve flow parameters.

Comparison with characteristics obtained directly from testing of actual hardware is, of course, required for ultimate verification of analytical results.

4. REFERENCES

1. Ahrendt, W. R., and Savant, C. J., Jr. — Servomechanism Practice, McGraw-Hill Book Co., Inc., New York, 1960.

2. Andreosky, E. — Functional Design of the Minuteman Flight Control System, Autonetics Division of North American Aviation, Inc.

3. Backus, F. I. — Describing Functions for Non-linear Electro-hydraulic Gimbaled Rocket-Engine Position Servos with Application to Closed-Loop Control Systems, General Dynamics Convair Report AE60-0287, June 1960.

4. Bonine, K. C. — Flight Dynamics and Control Analysis of the Atlas/Centaur Vehicle AC-5, General Dynamics Convair Report DDE65-004, January 1965.

5. Emerson, F. M. — Study of Systems for True Angle-of-Attack Measurement, WADC Technical Report 54-267, May 1955.

6. Hurley, M. J. — Advanced Flight Control System Functional Analysis, General Dynamics Convair Report GDC-ERR-AN-928, April 1966.

7. Leondes, C. T. — Guidance and Control of Aerospace Vehicles, UCLA Engineering Extension Lecture Series, Los Angeles, August 1961.

8. Lichtenstein, B. — "Gyros, Platforms, and Accelerometers," Technical Information for the Engineer, No. 3, Kearfott (General Precision), New Jersey, June 1963.

9. Lukens, D. R., Schmitt, A. F., and Broucek, G. T. — Approximate Transfer Functions for Flexible-Booster-and-Autopilot Analysis, General Dynamics Convair Report AE61-0198, April 1961.

10. Mitchell, J. L., and Peck, R. F. — An NACA Vane-Type Angle-of-Attack Indicator for Use at Subsonic and Supersonic Speeds, NACA Technical Note 3441, May 1955.

11. Savant, C. J., Howard, R. C., Solloway, C. B., and Savant, C. A. — Principles of Inertial Navigation, McGraw-Hill Book Co., Inc., New York, 1961.

12. Slater, J. M. — Inertial Guidance Sensors, Reinhold Publishing, New York, 1964.

13. Thayer, W. J. — Transfer Functions for Moog Servovalves, Moog Servocontrols TN103, January 1965.

14. Lewis, E. E., and Stern, H. — Design of Hydraulic Control Systems, McGraw-Hill Book Co., Inc., New York, 1962.

15. Blackburn, J. F., Reethof, G., and Shearer, J. L. — Fluid Power Control, MIT Press, Cambridge, Mass., 1960.

16. Greensite, A. — Design Criteria for Control of Space Vehicles, Vol. I, part 3, Trajectory Equations, General Dynamics Convair Report No. GDC-DDE65-058, 1 November 1965.

NASA-Langley, 1967 —— 31 CR-830

"The aeronautical and space activities of the United States shall be conducted so as to contribute . . . to the expansion of human knowledge of phenomena in the atmosphere and space. The Administration shall provide for the widest practicable and appropriate dissemination of information concerning its activities and the results thereof."

—NATIONAL AERONAUTICS AND SPACE ACT OF 1958

NASA SCIENTIFIC AND TECHNICAL PUBLICATIONS

TECHNICAL REPORTS: Scientific and technical information considered important, complete, and a lasting contribution to existing knowledge.

TECHNICAL NOTES: Information less broad in scope but nevertheless of importance as a contribution to existing knowledge.

TECHNICAL MEMORANDUMS: Information receiving limited distribution because of preliminary data, security classification, or other reasons.

CONTRACTOR REPORTS: Scientific and technical information generated under a NASA contract or grant and considered an important contribution to existing knowledge.

TECHNICAL TRANSLATIONS: Information published in a foreign language considered to merit NASA distribution in English.

SPECIAL PUBLICATIONS: Information derived from or of value to NASA activities. Publications include conference proceedings, monographs, data compilations, handbooks, sourcebooks, and special bibliographies.

TECHNOLOGY UTILIZATION PUBLICATIONS: Information on technology used by NASA that may be of particular interest in commercial and other non-aerospace applications. Publications include Tech Briefs, Technology Utilization Reports and Notes, and Technology Surveys.

Details on the availability of these publications may be obtained from:

SCIENTIFIC AND TECHNICAL INFORMATION DIVISION

NATIONAL AERONAUTICS AND SPACE ADMINISTRATION

Washington, D.C. 20546